

ENGINEERING DEVICE PLATFORMS FOR MICROPHYSIOLOGICAL
MODELING OF MULTI-ORGAN EFFECTS IN CANCER

AN ABSTRACT

SUBMITTED ON THE FIFTH DAY OF MAY 2022

TO THE DEPARTMENT OF BIOMEDICAL ENGINEERING

IN PARTIAL FUFULIMENT OF THE REQUIREMNETS

OF THE SCHOOL OF SCIENCE AND ENGINEERING


OF TULANE UNIVERSITY

FOR THE DEGREE

OF

MASTERS OF SCIENCE IN ENGINEERING

BY

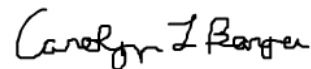


GABRIELLE FORTES

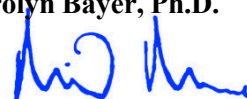
APPROVED BY:



Mark J. Mondrinos, Ph.D.
Advisor



Carolyn Bayer, Ph.D.



Michael J. Moore, Ph.D.

ABSTRACT

This research aims to develop microphysiological models for studying pathophysiology across multiple organ types with an emphasis on cancer. The primary design considerations are to enable the culturing of multiple tissue/organ types and establish fluidic interconnectivity to facilitate chemical communication between them. Engineering individual organ compartments with relevant physiological functions is a basic requirement for multiorgan models. However, to fully capture organism physiology, a multi-organ model must allow transport to occur through a living vascular endothelium. This thesis presents the engineering and validation of two separate multi-organ devices platforms. The first device features a multilayer configuration that uses membranes to separate channels and compartments. The multilayer device is a simple implementation that achieves the goal of intercellular communication between organ compartments. The second device features a membrane-free design that enables cell transit between adjacent channels and chambers in a horizontal configuration. The membrane-free devices achieve the goal of enabling physiological (perfusable) vascularization in the system.

A digital manufacturing-based workflow previously established in our lab enabled rapid prototyping and design iteration. Primary contributions of this thesis include optimizing the designs of these MPS models for future use by reaching almost 100% loading success rates and establishing standardized workflows for device fabrication that address inherent limitations of our equipment. Following the reduction to practice phase, both device platforms were used to establish a prototype MPS model of cancer cachexia, which is driven by tumor inflammation. This thesis work established tissue engineering methods for interfacing a lung cancer module with three placeholder stromal-vascular tissues. We used ICAM-1 as a marker of vascular inflammation and tested the hypotheses that cancer will induce vascular inflammation in the model and that the effect will be a function of distance from the tumor module in the device. This thesis establishes a foundation for more complex implementations with representative organ modules incorporated such as muscle, liver, and adipose tissue and complete vascularization.

ENGINEERING DEVICE PLATFORMS FOR MICROPHYSIOLOGICAL
MODELING OF MULTI-ORGAN EFFECTS IN CANCER

A THESIS

SUBMITTED ON THE FIFTH DAY OF MAY 2022
TO THE DEPARTMENT OF BIOMEDICAL ENGINEERING
IN PARTIAL FUFULIMENT OF THE REQUIREMNETS
OF THE SCHOOL OF SCIENCE AND ENGINEERING
OF TULANE UNIVERSITY

FOR THE DEGREE

OF

MASTERS OF SCIENCE IN ENGINEERING

BY

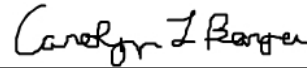


GABRIELLE FORTES

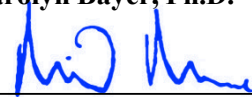
APPROVED BY:



Mark J. Mondrinos, Ph.D.
Advisor



Carolyn Bayer, Ph.D.



Michael J. Moore, Ph.D.

© Copyright by Gabrielle Fortes

2022 All Rights Reserved

Acknowledgments

I would like to thank Dr. Mark Mondrinos for the constant support and trust he has put into my work within the lab. I would also like to thank Dr. Ethan Byrne, Michael Conrad, and Elisabet Olsen for helping me overcome the numerous issues I encountered during this journey. I would finally like to thank all of the TEMPS lab for helping me keep a smile on my face and Tulane's Department of Biomedical Engineering for providing the resources necessary to further my education.

List of Figures

Figure 1.....	4
Figure 2.....	18
Figure 3.....	20
Figure 4.....	22
Figure 5.....	25
Figure 6.....	30
Figure 7.....	30
Figure 8.....	32
Figure 9.....	32
Figure 10.....	34
Figure 11.....	35
Figure 12.....	36
Figure 13.....	38
Figure 14.....	40
Figure 15.....	41
Figure 16.....	42
Figure 17.....	43
Figure 18.....	45
Figure 19.....	46
Figure 20.....	47
Figure 21.....	47
Table 1.....	44

TABLE OF CONTENTS

CHAPTER ONE: INTRODUCTION

1.1 Multi-Organ Pathophysiology	1
1.2 Cancer	1
1.3 Tumor Microenvironment	2
1.4 Vascular Inflammation	3
1.5 Cancer-Induced Cachexia	3
1.6 Modeling Multi-organ Effects of Cancer	5
1.7 Engineering a Tumor Microenvironment.....	6
1.8 Vascular Development and Physiology	7
1.9 Engineering a Vascular Network.....	9
1.10 Multi-Organ Modeling.....	10
1.11 Microphysiological System.....	12

CHAPTER 2: MATERIALS AND METHODS

2.1 Research Design and Goals.....	14
2.2 Master Mold Fabrication.....	15
2.3 Post-Print Mold Processing.....	16
2.4 Clear Coating	16
2.5 PDMS Soft Lithography.....	17
2.6 PDMS Replica Molding.....	17
2.7 Multi-Organ Membrane Design	18
2.8 Multi-Organ Membrane-Free Design	20
2.9 Membrane-Free Device Assembly.....	23
2.10 Membrane Device Assembly	24
2.11 Device Preparation for Biological Experiments.....	25
2.12 Injection Testing.....	26
2.13 Cell Culture	26
2.14 Vasculogenic Hydrogel.....	26
2.15 Device Loading.....	27
2.16 Assessment of Cell Viability	27
2.17 Staining and Microscopy.....	28
2.18 Image Analysis.....	28
2.19 Statistical Analysis	28

CHAPTER 3: RESULTS

3.1 Multi-organ Membrane Device V1	30
3.2 Multi-organ Membrane Device V2	30
3.3 V2 Media Consumption Calculations	33

3.4 Multi-organ Membrane Device V3	33
3.5 Multi-organ Membrane-Free Device	37
3.6 Moving Away from Replica Molding.....	37
3.7 The Effects of Spray Coating.....	38
3.8 Improving Gel Anchorage.....	40
3.9 Membrane-Free Device Iterations.....	42
CHAPTER 4: DISCUSSION AND CONCLUSIONS	
4.1 Digital Manufacturing-Based Organ Chip Fabrication.....	50
4.2 Design Constraints of Membrane Devices for Media Consumption.....	52
4.3 Vascular Formation in Organ Compartments	53
4.4 Vascular Inflammation and ICAM Expression.....	53
4.5 Conclusions and Future Work.....	54
LIST OF REFERENCES	57

CHAPTER ONE: INTRODUCTION

1.1 Multi-Organ Pathophysiology

Most, if not all, pathologies are based on physiological interactions between various organ systems. These interactions occur through the release of soluble factors from the primary site of the pathology. The signals elicit an effect both on local tissues (paracrine signaling via diffusion through a cell's extracellular matrix) and distant tissues (endocrine signaling via the circulatory system). Further, these signals can be amplified through immune cells and signal transduction cascades. A canonical example of this phenomenon is sepsis-induced acute respiratory distress syndrome (ARDS). When an external injury or infection induces sepsis, there is an influx of inflammatory cells (macrophages, neutrophils, etc.) into the alveoli which cause it to fill with a plasma exudate. The severe inflammatory response incites swelling and necrosis of capillary endothelial cells, which increases the permeability of the pulmonary capillaries. This results in acute pulmonary edema and ARDS. If not treated fast enough, sepsis-induced ARDS can lead to lung failure and even death.^{1,23}

Many diseases at the forefront of scientific discovery-cancer, cystic fibrosis, obesity, diabetes, etc.- have a multi-organ physiological basis. To improve physiological relevance and therefore clinical translation, it is essential for researchers to incorporate multiple organ-tissue types within their disease models. It is equally important is for these models to enable physiologically relevant communication between the various organ components. This thesis will focus on developing two separate 3D modeling platforms to do just that.

1.2 Cancer

For this thesis, the main application of my multi-organ modeling platforms is to study cancer. Cancer is a complex pathology most notably characterized by unregulated cell

proliferation. A common misconception is that cancer is synonymous with a tumor. A tumor is a mass of cells that proliferates irregularly as a result of mutations or amplifications of protooncogenes. Alone, unregulated cell proliferation is not enough to promote metastasis and therefore, not every tumor can be classified as cancer.² Tumors that cannot metastasize are termed benign and are not considered cancer. Tumors with the capability to spread via the circulatory or lymphatic system are considered malignant and can be classified as cancer.

1.3 Tumor Microenvironment

Cancer cells release tumor-derived signals that induce cellular, molecular, and physical changes to nearby tissues. These interactions directly affect a tumor's ability to metastasize. An important component influencing metastasis is the cell's ability to secrete proteases that digest ECM components.² The ability to digest ECM decreases a cancer's adhesion, allowing it to infiltrate surrounding tissues. Another major factor is a cancer cell's ability to produce growth factors to encourage proliferation. The surrounding tissue tumor cells interact with is termed the tumor microenvironment (TME). Composition varies with tumor type, but the main components are stromal cells, vasculature, lymphatics, immune cells, and extracellular matrix (ECM). Immune cells such as T cells, B cells, neutrophils, and macrophages are a big player in the TME as they inhibit adaptive immunity and secrete growth factors. M2 macrophages are especially important for their role in suppressing immune response and secrete vascular endothelial growth factor (VEGF-A) to promote vessel formation. The main stromal cells in the TME include fibroblasts, adipocytes, vascular endothelial cells (EC), and stellate cells. Vascular ECs play a critical role in tumor progression by facilitating nutrient/waste transportation and angiogenesis. They secrete pro-angiogenic factors like VEGF and platelet derived growth factor (PDGF). ECs, adipocytes, stellate cells, and pericytes all have the ability to transform into cancer-associated fibroblasts (CAFs). CAFs produce ECM, cytokines, and growth factors like TGF- β that promotes epithelial-mesenchymal transition and angiogenesis.³

1.4 Vascular Inflammation

Another important component of cancer metastasis is vascular inflammation. With vascular inflammation, luminal endothelial adhesion proteins, such as intercellular adhesion molecule (ICAM1), are upregulated to encourage leukocyte adhesion to endothelial cells. This phenomenon is paired with the diminishing of endothelial junctional adhesions allowing for leukocyte transmigration. During tumor progression, inflammatory cytokines released in the TME such as IL1- β and TNF- α encourage vascular inflammation. Similarly, to leukocytes, the dysregulated barrier function allows circulating cancer cells to adhere to endothelial cells and transmigrate to a secondary location.⁴ Vascular inflammation will be used to validate organ-to-organ signaling during the testing phase of my modeling platforms.

1.5 Cancer-Induced Cachexia

Another important multi-organ interaction associated with cancer is cachexia. Cachexia is a metabolic wasting disorder that occurs in roughly 80% of advanced malignancy cancer patients. Cachexia is also known to occur in earlier stages of certain cancers such as pancreatic. This disorder is characterized by extreme weight loss, fatigue, and metabolic dysfunction. There is a clear clinical link between cachexia and cancer metastasis. Yet, many questions are still unanswered regarding the pathophysiological pathways that connect the two. What is known is that tumor secreted factors and systemic inflammation lead to an energy imbalance through an increase in metabolic energy consumption and decrease in energy uptake.

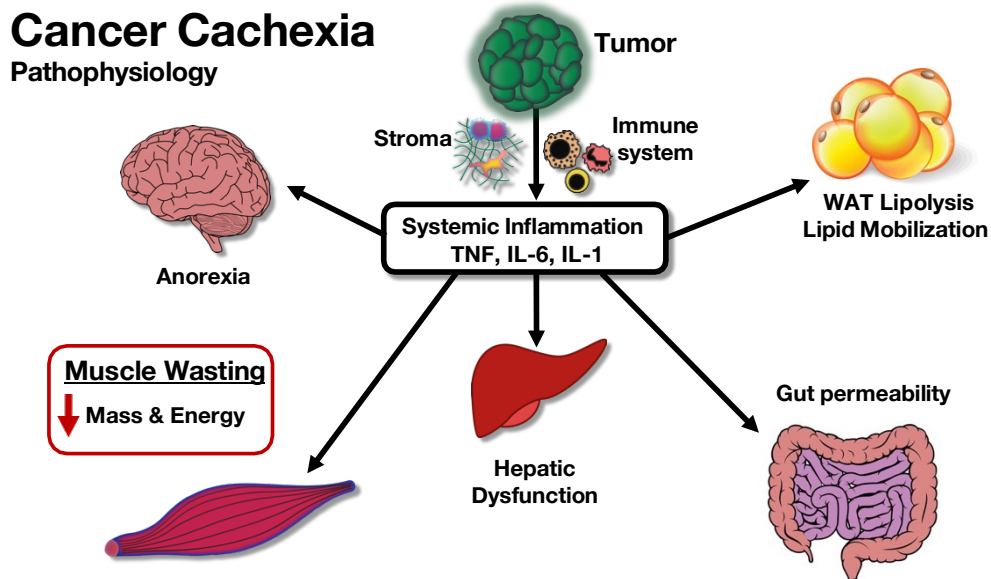


Figure1: Multi-Organ Effects of Cancer-Induced Cachexia

Effects of cachexia can be seen throughout most organ system of the body. In the liver, we see energy wasting associated with metabolic futile cycles. The prime example of this is the switch to gluconeogenesis through the Cori cycle. Cachexia also activates the liver acute phase response and hypertrophy.⁵ In the GI tract, we see gut barrier dysfunction and intestinal malabsorption. In the stomach, we see reduced food intake due to nausea, mechanical dysfunctions, and an increased resistance to ghrelin. Cachexia has also been associated with inflammation of the CNS and the induction of anorexia. In adipose tissue, lipolysis and thermogenesis are elevated. Lastly, in cardiac and skeletal muscle, there is an increase in proteolysis, insulin resistance, and a decrease in protein synthesis associated with cachexia.⁶

Though the disruptions in functional outputs are understood, the mechanisms underlying cachexia are largely understudied. Filling this need was the primary motivation for developing my multi-organ platforms. It is important to note this thesis only covers the initial development of the multi-organ models and not the specific application to modeling cachexia. A long-term goal

of our lab is to eventually use these models to study the complex interactions of energy-wasting processes associated with cancer-induced cachexia.

1.6 Modeling Multi-organ Effects of Cancer

Now that the physiological basis of organ-to-organ communication and cancer pathology has been explored, I will discuss the necessary components and considerations for engineering an in-vitro multi-organ model to study the effects of cancer. The most essential component is incorporating the cancer tissue itself and something to model the tumor microenvironment. This can be accomplished by mimicking the structure or primary biological components of the TME. Next is the vasculature. Vasculature makes up bulk tissue of all organ types in addition to the tumor microenvironment. Therefore, it should be incorporated across all tissue components. Inclusion of vasculature is essential to replicate the transportation of nutrients, waste, and tumor-secreted signals within the model. The vasculature should facilitate transport within the individual tissues in addition to facilitating transport between the various organ types. To function properly, it is necessary for the vasculature to mimic the physiological structure of blood vessels. At a minimum, the vasculature should have a lumen structure surrounded by a permeable barrier structure. Physiological relevance would be further improved if the vasculature could interact with nearby tissues and signals such as with vascular inflammation.

Because the models developed in this thesis are meant to study the interactions between organs, the important consideration is to incorporate multiple organ types. Various organ types and their environments should be distanced from the tumor to mimic endocrine signaling. It is also essential for there to be some sort of connection between the different organ compartments. Without this connection, organ-to-organ signaling could not occur.

For modeling cachexia specifically (a future goal of our lab) it would be important to include liver, muscle, and fat tissue. The muscle and fat tissue could be looked at for degradation and endocrine changes, while the liver could be looked at for metabolic cycle changes. Another

important application is modeling pre-metastasis. The distant organ environments would contain stromal and interstitial tissue to simulate pre-metastatic conditioning. This model is not the focus of my thesis but is currently under development in our lab.

1.7 Engineering a Tumor Microenvironment:

As discussed previously, the tumor microenvironment plays a significant role in promoting tumor progression and metastasis. Therefore, it is no surprise a major focus of recent tissue engineering literature has been engineering tumor microenvironments. The most prominent in-vitro cancer models are 2D cultures of immortalized cell lines. Cell lines are most commonly epithelial cancer cells such as A549. These traditional models have poor clinical translatability due to their homogeneity and lack of biophysical and biochemical environmental cues.⁷ On the other hand, 3D in-vitro tumor models enable the integration of multiple cell types, mechanical stimulation through fluid flow, 3D extracellular matrix, and biochemical gradients which better emulate the pathophysiological interactions of the tumor and its microenvironment.

Prime examples of 3D tumor cell culture include spheroids and organoids. Spheroids are multi-cellular, spherical clumps of cells that promote cell-to-cell adhesion. Multiple studies have shown that larger spheroids can form proliferative and necrotic zones that induce biological Gradients.⁸ Another study even suggested that spheroid cultures have an altered drug sensitivity through increased expression of drug-resistant genes.⁹ Organoid cancer cultures are usually patient derived or pluripotent stem-cell derived cell aggregates. They are the most suitable culture form for patient-specific 3D in-vitro modeling. However, cellular composition may alter with time making standardization difficult.

There are a variety of biomaterials to consider for seeding cancer cells into a 3D in-vitro model. Biomaterials imitate the biophysical and composition of ECM with certain limitations. Certain biomaterials, such as Matrigel, lack the structural properties of the materials seen in vivo. In addition, biomaterials contain cytokines and growth factors that can directly influence cell

behavior.¹⁰ Many of the limitations of biomaterials can be evaded by using individual ECM components such as collagen and fibrin. Interestingly, collagen is known to promote more aggressive phenotypes when compared to Matrigel.¹⁰ A major benefit of collagen as a base for hydrogels is it also enables easy tuning of its structural and mechanical properties. This allows spheroids to easily be seeded within a collagen-base hydrogel which was part of the reason I chose this biomaterial as the framework for each individual tissue compartment.

Many research groups have also incorporated vasculature and stromal cells into their engineered tumor microenvironments. One approach to doing this is to seed cancer cells into a vascularized hydrogel. Roger Kamm's lab has been at the forefront of this vascularized hydrogel technology. In one paper, they modelled tumor extravasation by seeding human umbilical vein endothelial cells (HUVECs) and human lung fibroblasts (HLFs) into adjacent fibrin-based hydrogels. The HUVECs self-assembled into a perfusable vascular network by Day5.¹¹ An adaptation of this protocol was used to incorporate vascularized hydrogels into my tissue compartments.

Other factors to consider for improving the pathophysiological relevance of TME models is the incorporation of immune cells and mechanical stimulation. Given the limited timeline of this thesis and the fact that the device platforms are at an early stage of development, these components were not incorporated into my models' tumor microenvironment.

1.8 Vascular Development and Physiology

The vascular system is a network of vessels responsible for maintaining cellular homeostasis. This is accomplished through the transportation of blood, oxygen, nutrients, and waste to and from tissues/organs via such vessels. Blood vessels also facilitate endocrine cellular communication by transporting signaling molecules. While previous sections explored the role of vasculature in tumor growth and metastasis, this section will focus on vascular cell biology and development. Understanding such information is critical for engineering a functional vascular network.

The composition of blood vessels varies based on size. The smallest blood vessels, capillaries, are composed of endothelial cells, a basal lamina, and a low number of pericytes. The largest vessels of the body, arteries and veins, are composed of connective and smooth muscle tissue layers in addition to ECs and stromal cells. ECs form the thin inner lining of a vessel lumen. ECs are connected to a basal lamina and facilitate the barrier function of blood vessels (as discussed early in the vascular inflammation section). Another important function of ECs is to repair, maintain, remodel, and expand blood vessels. ECs adapt vasculature to meet the environmental needs facilitated by VEGF and other cues such as flow-induced shear stress. Stromal cells associated with vasculature include fibroblasts and pericytes. Pericytes are mural cells that wrap around blood capillaries. They are responsible for stimulating the assembly of the basement membrane matrix and are recruited through the release of PDGF- β by endothelial cells.¹² The main function of fibroblasts is to maintain and synthesize the extracellular matrix. Fibroblasts also promote angiogenesis by secreting growth factors including VEGF, TGF- β , and PDGF.¹³

There are three distinct processes encompassing vascular network development: vasculogenesis, angiogenesis, and arteriogenesis. Vasculogenesis refers to the de novo formation of blood vessels occurring during embryonic development and wound healing. Vasculogenesis during embryonic development occurs when angioblasts differentiate into endothelial cells and migrate to create the primary capillary plexus.¹⁴ Angiogenesis refers to the intussusception and sprouting of new branches from preexisting vessels. Angiogenesis occurs during embryonic development, wound healing, and inflammation. Hypoxic conditions associated with injury cause an upregulation of hypoxia-inducible factor 1 (HIF-1). This leads to an increase in VEGF and endothelial cells respond by remodeling the damaged tissues.¹¹ Angiogenesis is responsible for extending capillary networks. Arteriogenesis, also known as collateral growth, refers to the remodeling of preexisting arterio-arteriolar anastomoses into fully functional arterioles.¹⁵ Arteriogenesis is associated with an increase in diameter of preexisting vessels and

is often initiated in response to physical forces such as an alteration in shear stress or an occlusion of the vessel. Also associated with arteriogenesis is anastomosis, which is the formation of a connection between existing blood vessels. Anastomosis is essential for perfusability and has been a focus of study in our lab.

1.9 Engineering a Vascular Network

There are a variety of factors contributing to vascular homeostasis that have shown to be important for engineering blood vessels. The first is having the proper balance of angiogenic factors such as VEGF, FGF and angiopoietin. VEGF is responsible for the regulation of tubulogenesis, while FGF is responsible for the proliferation of the endothelial cells.¹⁶ Angiopoietin triggers endothelial cell sprouting.¹⁴ These angiogenic factors can be incorporated into a model through media supplementation or by including cell types that secrete these factors. However, culturing ECs with angiogenic factors is not sufficient for vascular formation. Hughes et al. found that ECs cultured with only angiogenic factors promoted some endothelial migration but not lumen formation. Yet, when ECs were co-cultured with fibroblasts, robust EC sprouting and lumen formation occurred.¹³ Fibroblasts have proven to be an essential component of engineering vascular tissue. As seen with wound healing, fibroblast secreted ECM components like collagen and fibronectin provide a temporary scaffold for ECs to invade and rearrange into the blood vessels. Fibroblast-derived matrix proteins also help facilitate the stiffness of vascular matrices. Only with an optimal stiffness will these vessels be able to adequately maintain pressure and blood flow as shown in studies by Newman et al. Fibrin has become a standard component of promoting vascularization in hydrogels. In the Kamm paper, for example, fibrinogen was converted to fibrin using thrombin, which was used to see HUVECs and HLFs into a microfluidic device to form a vascular network for tumor extravasation.¹¹

Another important consideration for engineering vasculature is the effect of mechanical stimuli. Interstitial flow, in particular, is known to cause shear stress on endothelial cells that acts as a stimulus for vascular growth and homeostasis by releasing biomolecular signals. In a study from Kim et al, only when interstitial flow was introduced into the microfluidic platform did endothelial sprouts form. This study also found that when the direction of flow was opposite of sprouting, almost double the number of endothelial sprouts were formed. Further, studies have found that laminar flow activates downstream anti-inflammatory pathways while, the disruption of flow activates proinflammatory pathways. Flow is also important for regulating the release of nitric oxide necessary for paracrine signaling.

1.10 Multi-Organ Modeling

There are a variety of applications for multi-organ modeling, the most essential being the study of systemic/chronic diseases and drug discovery. The ability for animal models to capture full-body physiology has pushed them to the front line of multi-organ modeling. Yet, there are numerous limitations to animal models that make clinical translation difficult. This is especially evident in the realm of drug discovery, where 40% of drugs that succeeded in the animal trial phase fail during clinical trials. The biggest limitation of animal models is the bio-molecular differences that alter physiological responses and pathways. This can be exemplified by a study from the Stanford Genome Technology Center which compared the genomic inflammatory responses of murines and humans to different insults. They found the Pearson correlation for genetic changes associated with human and mouse burns was only 0.08. For human and mouse trauma, the Pearson correlation was only 0.05. Even more disturbing, there was a 0.00 Pearson correlation in genetic changes associated with human endotoxemia and mouse endotoxemia.¹⁷ In the context of drug discovery, the physiological differences between humans and other species often leads in inaccurate prediction of human toxicity. The asthma drug Isuprel, for example,

killed over 3,500 people in Great Britain. Yet, no toxicity to the compound was observed in rats, dogs, monkeys, and guinea pigs.¹⁸ Other limitations of animal models include lack of reproducibility, low throughput, lack of experimental control, cost, and concerns with ethical considerations.

The biomolecular differences seen with animal models implies that human cell-based modeling platforms may be necessary to improve clinical translatability. Standard 2D cell culture approaches eliminate the phylogenetic differences of animal models and have high throughput. However, they lack the physiological form and function to properly model most in-vivo interactions. Developments in 3D tissue engineering such as hydrogels, tissue scaffolds, and organoids allow for more accurate recapitulation of physiological structure and function of individual organs. However, standard 3D tissue engineering approaches do not support the interactions between multiple organ types as seen within the body. This is where microphysiological systems come in to play.

Microphysiological systems (MPS) are platforms that combine microfluidics and 3D tissue engineering for studying diseases and drug development. MPS work to bridge the gap between standard tissue culture techniques and whole organism physiology by incorporating the key features of organ-specific architectures and functions along with biophysical cues into a highly controlled, interconnected system. MPS are also known as organ-on-a-chip systems or organ chips. One of the first organ-chips came in 2010 from the Ingber group at Harvard with their Lung-on-a-Chip model. Their system modeled the alveoli-capillary interface of lungs by co-culturing alveolar and capillary cells between a porous membrane connected to a vacuum to simulate breathing movements.¹⁹ Since then, the MPS field has grown exponentially with platforms emerging to model almost every organ in the body. The ultimate goal of the organ chip field is to one day develop a

“body-on-a-chip” in which every organ system is represented within one device. The concept of body-on-a-chip originated from pharmacology, specifically to assess drug toxicity and absorption, distribution, metabolism, and elimination (ADME) processes across all organs. Early papers from the Shuler group were major propagators of the body-on-a-chip concept. One example is his Microscale Cell Culture Analog (μ CCA) developed back in 2008. The device was one of the first of its kind to culture multiple organ constructs simultaneously. Liver, bone marrow, cancerous, and multi-drug resistant cancer cells were all cultured on μ CCA for evaluating different drug compounds.²⁰ Since then, Schuler has published a plethora of multi-organ MPS models including one with 14 different tissue chambers.²¹

1.11 Microphysiological Systems

There are a multitude of aspects associated with organ chip technology that address the limitations of animal modeling and standard 2D tissue culture. Microphysiological systems allow for a high degree of experimental control and enable the integration of fluidics, stimuli, and biological constructs for increased physiological relevance. A benefit of MPS over other modeling systems is the ability to manipulate the cell-to-liquid volume ratio. Microfluidic technology allows for a more physiologically relevant cell-to-liquid volume ratio than seen with standard cell culture. Although, there are limitations to this with static MPS culture as the cell-to-liquid volume ratio in the body is aided by multiple mechanisms of transport. These mechanisms include convection in the blood, diffusion in the tissue, and convection in the tissue via interstitial flow. Incorporating pumps into an MPS enables physiological mimicry. However, there

is a tradeoff between physiological relevance and usability. Static cultures are easier to implement and will be more readily adapted by non-expert users.

The ability to incorporate biomechanical stimuli such as flow with an MPS is another advantage of this modeling technique. Flow within an MPS is created using pumps or gravity driven mechanisms such as a rocker. The movement of fluids within an MPS increases convective transport. Convective transport is responsible for many important processes in the body, one of them being oxygen transport. As discussed earlier, mechanical stimulation is necessary for vascular maturation. Interstitial flow causes shear stress on ECs that stimulates vascular growth and homeostasis through biomolecular signals.^{21,26} The fluidics of an MPS system also allow for easy control of gradients and transport rates.²⁷. This is especially important for multi-organ models to facilitate communication of signals between them.

MPS multi-organ models are currently lacking in usability and reproducibility. Simplicity is needed for adoption by non-expert users. The motivation for my first modeling platform is to enable basic organ-to-organ communication to demonstrate how cancer affects cells in other parts of the body. The second modeling platform increases physiological relevance by enabling perfusable vascularization in a multi-organ system

Chapter 2: Materials and Methods

2.1 Research Design and Goals

This research aims to develop microphysiological systems to model the effects of a pathology across multiple organ types. The main considerations when designing these microphysiological systems are to enable the culturing of multiple tissue/organ types and establish fluidic interconnectivity to facilitate chemical communication between them. However, to fully capture organism physiology, a multi-organ model must allow transport to occur through a living vascular endothelium. This design goal builds off the following criteria:

1. Bulk vascularization of 3D tissue in compartments
2. Interfaces enabling free movement of cells between compartments
3. Conditions that facilitate vascular anastomosis
4. Promotion of vascular maturation

Two separate microphysiological modeling platforms were developed to address the first and second criteria respectively. The goal with my first device was to create a biologically simple, yet robust modeling platform that incorporates the vascularization of multiple tissue compartments. This was accomplished using vertically configured membrane device. The second multi-organ modeling platform focused on increasing physiological relevance by removing physical membrane barriers to enable cell transit. This was accomplished using surface-tension based membrane-free technology.

A digital manufacturing-based workflow previously established in our lab enabled rapid prototyping and design iterating of the modeling platforms. Much of the work involved in this thesis was in optimizing the designs of these MPS models and optimizing

the workflow for fabricating them. The other portion of this thesis was running biological experiments with the MPS devices to answer basic physiological questions. The primary focus of these biological experiments was to explore how signaling from a cancer chamber elicits effects in the other non-tumor tissue chambers.

2.2 Master Mold Fabrication:

Master molds for the organ chips were fabricated using a consumer level stereolithography (SLA) printer. Molds were digitally constructed with CAD software, specifically SolidWorks and Fusion360. The molds were extruded with positive features that complement to negative features on the organ chip layer after PDMS soft lithography. The files were exported in a .stl format to PreForm, Formlab's pre-print setup software. Using this software, the molds were oriented with features facing upwards, parallel to the print platform. In addition, supports of touchpoint size 0.60mm and density of 1.20 were added. These files were then uploaded to a Formlab Form 3 SLA 3D Printer and printed using Formlab's clear resin. After printing, the print platform containing the molds was immersed into a tank of isopropyl alcohol and hand agitated to remove excess liquid resin. The print platform was then inserted into the Formlab's FormWash machine and washed for 20 minutes. Prints were then removed from the print platform and the hand agitation step was repeated. Molds were left out to dry near a fan for a minimum of 45 minutes before being UV cured at 60°C for 20 minutes in Formlab's FormCure.²⁹ Mold supports were left on throughout the entire process to ensure stability and easy handling.

2.3 Post-Print Mold Processing

To achieve compatibility of the SLA printed master molds with PDMS soft lithography, a sequence of post-processing steps was established to tune the mold surface properties. After curing, the molds were placed in an oven at 130°C for 2.5 hours. This “baking” process allows trapped volatiles from the resin to escape. If baking of the molds is not done, PDMS during the soft lithography process will not cure properly. Exposing the molds to the curing and baking process causes extreme deformation of the mold base. This phenomenon can be counteracted by flattening the molds between two heated 4x4x0.75in jeweler’s blocks. The flattening process is achieved by sandwiching a single mold between the jeweler’s blocks and slightly tightening a clamp around the stack for 30 minutes or until room temperature has been reached. Visual inspection is necessary to ensure the mold is centered properly between the two blocks. It is also important to orient the features of the molds upwards to avoid sagging of the features. Certain molds were coated in an automotive clear coat before undergoing silane treatment (Silanization Solution 1, Sigma Aldrich) for 1 hour in a desiccator.

2.4 Clear Coating

To address surface imperfections that make PDMS appear opaque after curing, certain molds were covered with a thin layer of automotive clear coat. To prepare for clear coating, lacquer thinner was poured into the molds, let sit for a minute, and aspirated out. The molds were placed in front of a fan to dry for 15 minutes. Within a fume hood, molds were oriented vertically and subjected to an automotive clear coating solution via airbrush. The clear coating solution was created using a 4:1 ratio of Sherman Williams Finish 1 FC720 Clear Coat to FH612 Hardener. The airbrush used was a Badger Air Brush Co. Model 105 Patriot Fine Gravity Airbrush. The airbrush was

attached to an air compressor with clear coating solution poured into the airbrush reservoir. The airbrush was held 6 to 10 inches away from the mold and perpendicular to the face containing mold features. Initially, a thin coat was applied by using consecutive horizontal passes until the entire face was covered. This was followed by vertical passes of the same nature. Molds were periodically rotated 90° degrees, and vertical/horizontal passes were repeated until a clear, completely uniform glossy affect was achieved. Clear coated parts were put in petri dishes to dry overnight at room temperature.

2.5 PDMS Soft Lithography

Individual organ chip layers were fabricated from polydimethylsiloxane (PDMS) using standard soft lithography. PDMS was prepared in a 10:1 weight ratio of DOWSIL 184 Silicone Elastomer Base to DOWSIL 184 Silicone Elastomer Curing Agent. After thoroughly mixing, the PDMS was degassed in a vacuum desiccator until all air bubbles had dissipated. The PDMS was then poured into the processed 3D printed molds and degassed again in the desiccator for roughly 30 minutes. A 3x2" glass slide was gently placed across the surface of the PDMS, careful not to form any bubbles. Then a jewelers block was placed on top each mold, and they were left to cure in an oven at 60°C for a minimum of 3 hours. This step is essential to ensure a perfectly flat surface for each device layer. After curing, the organ chip layers were removed from the molds and wrapped in packaging tape to minimize dust accumulation.

2.6 PDMS Replica Molding

The bottom layer of V0 of the octagon contains positive guide structures which function to enable gel pinning. To fabricate a PDMS layer patterned with positive features using soft lithography, a master mold with negative features must be poured. One limitation of our SLA 3D printer is its low resolution for patterning negative features

on the milli-scale. Therefore, replica molding was used to fabricate this layer. An SLA-printed master mold containing a positive border and features was poured using the above-described soft lithography process. The product of this initial pour is a PDMS “replica” mold containing the corresponding negative features. This “replica” mold was silane treated for 1 hour and poured again with PDMS, the outcome being an organ chip layer patterned with the appropriate positive guide structures. After curing for a minimum of 3 hours at 60° C, the PDMS layers were removed from the “replica” mold and wrapped in tape.

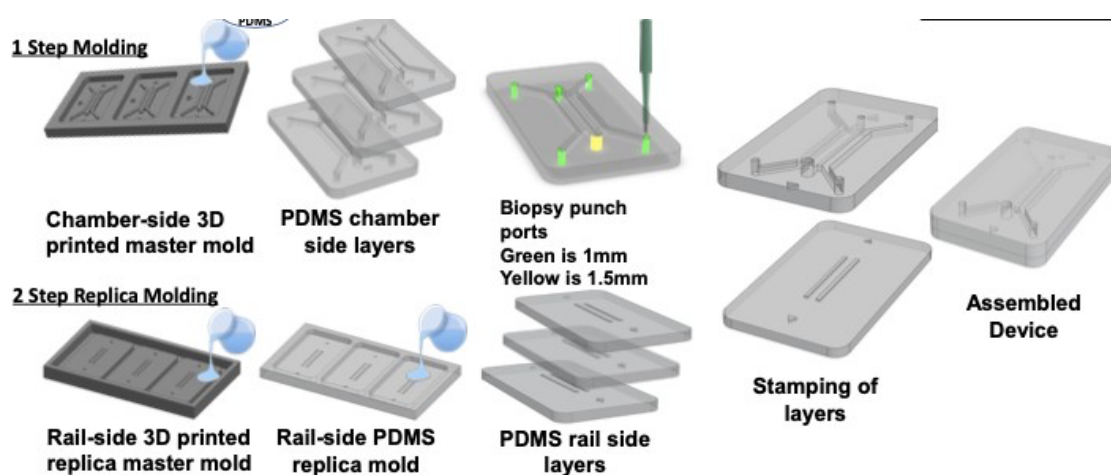


Figure 2: Replica Molding Soft Lithography vs. Standard PDMS Soft Lithography with Master Mold²⁵

2.7 Multi-Organ Membrane Device Design

.Most classic organ-on-a-chip systems, both in research and commercialized settings, are oriented in a vertical configuration. Vertically oriented devices have channels/features that are stacked on top of each other and separated by a semi-porous

membrane. Fluids within the system can perfuse throughout the various layers regulated by hydrostatic pressure differentials. Vertically oriented devices are robust and have a high rate of loading success.

The first multi-organ modeling platform, referred to as the “membrane device”, is based on this vertical design configuration. As mentioned previously, the goal of the this first device was to culture multiple vascularized tissue constructs and enable communication between them. To accomplish this, the top or “chamber” layer of the membrane device was designed to have four separate compartments to represent individual organs or tissue constructs. The bottom or “serpentine” layer contains a shared media channel that connects each of the organ compartments and enables communication. These layers are separated by a semi-porous membrane to facilitate transport between the compartments and media channel.

The ovular “organ” chambers within the top layer were cut extruded through the thickness of the device. This allows for an interface between the organ compartments and the membrane/shared media channel below. The exposure of the top of the chambers allows for easy loading of hydrogels to represent tissue constructs. The chambers also serve as individual media reservoirs to meet the consumption needs of each incorporated tissue type. The chamber layer also contains two cut extruded reservoirs to serve as media inlets and outlets connected to the shared media channel below. The bottom layer containing the shared media channel was designed in a serpentine configuration. This was done to increase residence time of the media in contact with each organ chamber.

Each mold contains 3 individual device layers, allowing for increasing fabrication through-put. Rapid fabrication was essential for testing and the iterative design process.

Design #1: Multi-Organ Membrane Device

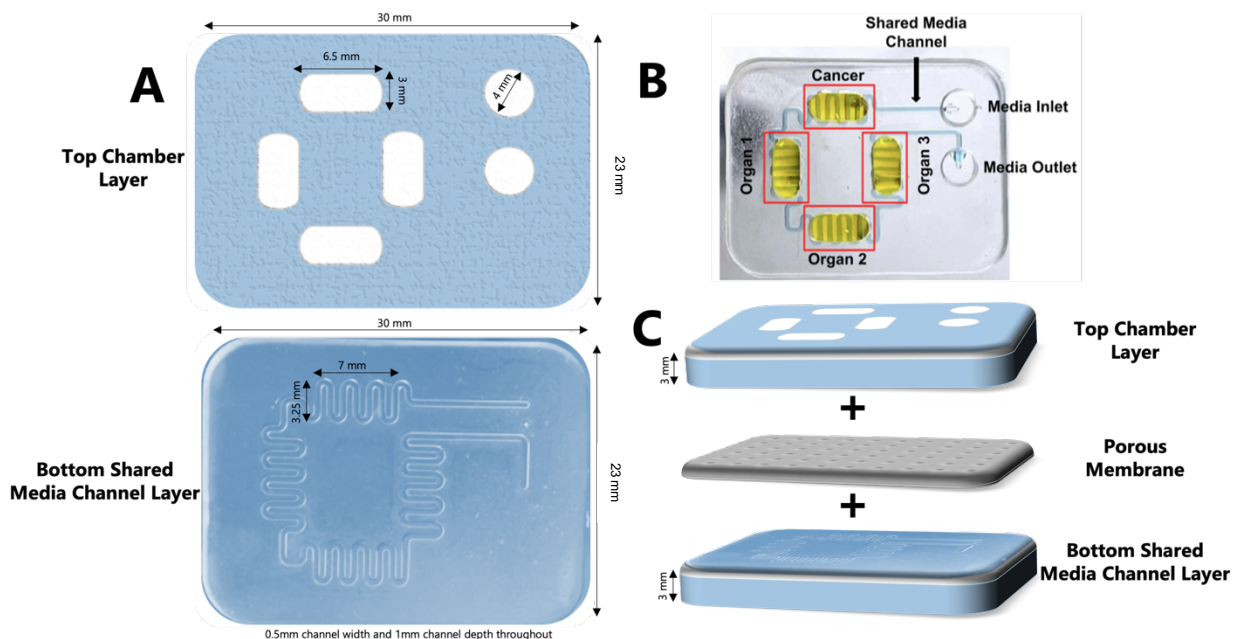


Figure 3: Multi-organ membrane free device design and dimensions. A) Top-down view of disassembled layers. B) Picture of an assembled device injected with food dye. C) Exploded view of individual device layers and their assembly.

As shown in part B of the figure above, the membrane device has the capacity to culture multiple organs within one system. It is important to note that for this thesis, vascularized tissue constructs were substituted in place of multiple organ types. This model is still in early stages of development, so the goal was to show proof of concept.

2.8 Multi-Organ Membrane Free Device Design

The goal of the second multi-organ modeling platform was to further enable the development of functional vasculature by allowing cell transit between compartments. This was accomplished by removing the physical barriers at the interfaces of the tissues

using membrane free technology. The modeling platform will be referred to as the “membrane-free” or “octagon’ device.

In a membrane-free device, channels are oriented along one horizontal plane. The general organization of a membrane-free device is to have a central gel chamber sandwiched between two other channels. Geometric structures situated at each channel interface create surface tension that stops the gel from pooling over into the side channels. Various iterations of this technology have been developed in recent *years*.²⁴ AIM Biotech, for example, was able to commercialize their micropillar technology into a whole product line of membrane-free organ chips.

Our lab has adopted the use of long rectangular, rail-like features we refer to as “guide-structures” to design membrane-free devices. An important parameter for functioning of the guide structures is to maintain a proper ratio of the height of the open interface between channels (h) and the overall height of the chamber (H). Previous work in our lab found that an $h/H=0.5$ has the highest success rate of gel injection.²⁵ My second device platform incorporates this membrane-free technology across four individual tissue compartments connected by a shared media channel.

Design #2: Multi-Organ Membrane-Free Device

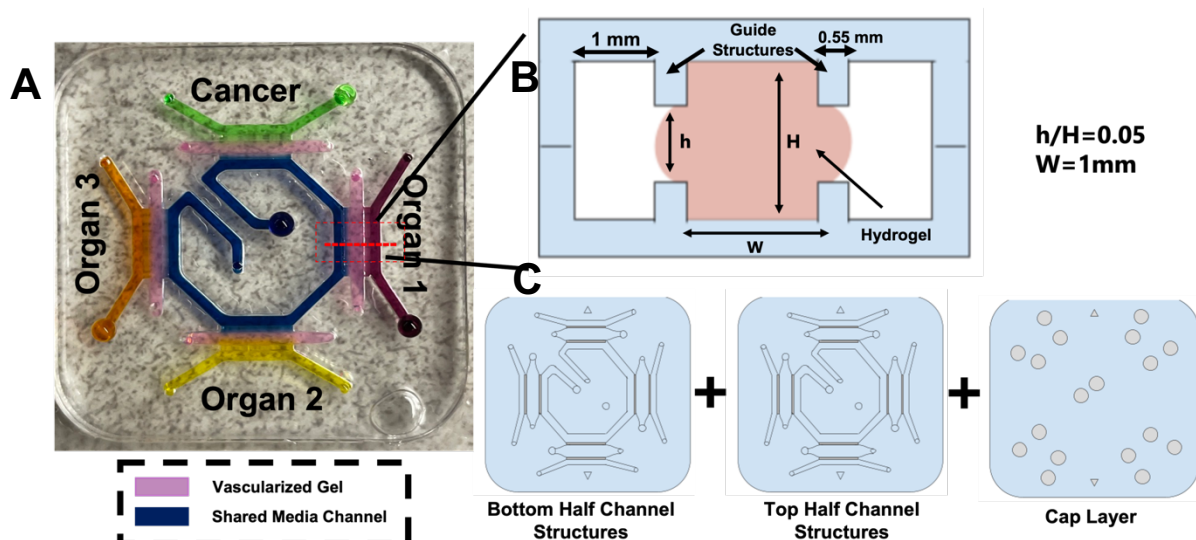


Figure 4: Overview of Multi-Organ Membrane-Free Device Design. A) Top view of assembled and food dye injected octagon device without the cap layer. B) Cross-sectional view of membrane-free technology within an individual organ compartment. C) Top views of individual device layers.

The multi-organ membrane-free device consists of three layers. The bottom and middle layers are patterned with exact halves of the gel chambers, media channels, and guide structures. They are identical with the exception of complementary alignment features represented as triangles on the diagram. The bottom and middle layer are sandwiched together with features facing to form channels within the device. The top or cap layer contains individual media reservoirs to support culture within the device. Each media reservoir connects to the inlets/outlets of individual media channels and gel chambers.

Each channel width is 1mm. The guide structures are 0.55mm in width and follow the h/H ratio of 0.5. In this device iteration, the total channel height is 1mm, which the guide structure heights are 0.25mm. The device is 42x42mm with filleted edges for easier bonding of device layers.

2.9 Membrane-Free (Octagon) Device Assembly

After fabricating the proper PDMS layers, biopsy punches were used to create access ports for the media channels, gel chamber, and media reservoirs. For the cap layer, a 4mm biopsy punch was used to puncture holes clean through to serve as the media reservoirs for the gels below. For the middle layer containing the gel chambers and media channels, a 1mm and 1.5mm biopsy punch were used. A 1mm hole was punched at one end of each gel chamber port, while a 1.5mm hole was punched at the other end of each gel port. This variation in hole size was incorporated to reduce resistance to flow during gel loading. In addition, 1mm holes were punched at each end of the media channels. An air compressor attached to an air gun was used to remove any excess PDMS from the hole punching and any accumulated dust.

The individual organ chip layers were bonded using PDMS stamping. An air compressor was connected to the Headway Research Inc.'s PWM50 Spin Controller. A dollar coin-sized dollop of freshly mixed and degassed PDMS was placed on top of a petri dish within the rotation chamber. The PDMS covered petri dish was spun at 1250 RPM for approximately one minute, leaving a thin, evenly spread layer of PDMS across the surface of the dish. The feature-containing face of the middle PDMS layer was placed down onto the PDMS covered petri dish. This layer was left to settle for roughly a minute, or until the PDMS spread across the entire PDMS layer face without filling into the patterned features. The middle layer was removed from the petri dish and placed face down onto the bottom PDMS layer. Light pressure was applied to ensure an even bond. This bonding process was repeated with the cap layer onto the non-featuring containing face of the middle layer, to create a full assembled device. The devices were left to cure at room temperature overnight. In the morning, the devices were moved to an oven to finalize curing at 60° for roughly 1 hour.

2.10 Membrane Device Assembly

The assembly process for membrane devices began by using a 4mm biopsy punch to remove excess PDMS underneath the media reservoirs of the cap layers. A hobby-grade scalpel was used to also remove any excess PDMS covering each of the 4 gel chambers within the cap layers. An air compressor attached to an air gun was then used to remove any PDMS fragments and dust on the PDMS layers. The layers were covered in packaging tape until time for bonding. The bottom layers containing the shared media channel were removed from the original glass slide and placed onto a clean one. Scissors were used to cut polyester semi-porous membranes (Sterlitech) slightly larger than the perimeter of the serpentine features. Fine-point tweezers were then used to place the membranes glossy side up onto the feature-containing face of the bottom, shared media channel layer. The membranes were aligned to fully cover each of the 4 serpentine channel features that come in contact with the gel chambers above. PDMS stamping as described earlier was then used to bond a cap layer onto the feature-containing face of the bottom, shared media channel layer. This process was repeated to add a second identical cap layer on top of the previous cap layer, making sure the features were properly aligned. Assembled devices were left to cure at room temperature overnight and placed in an oven at 60° for one hour the following morning to finish curing.

Organ-on-a-chip Device Fabrication

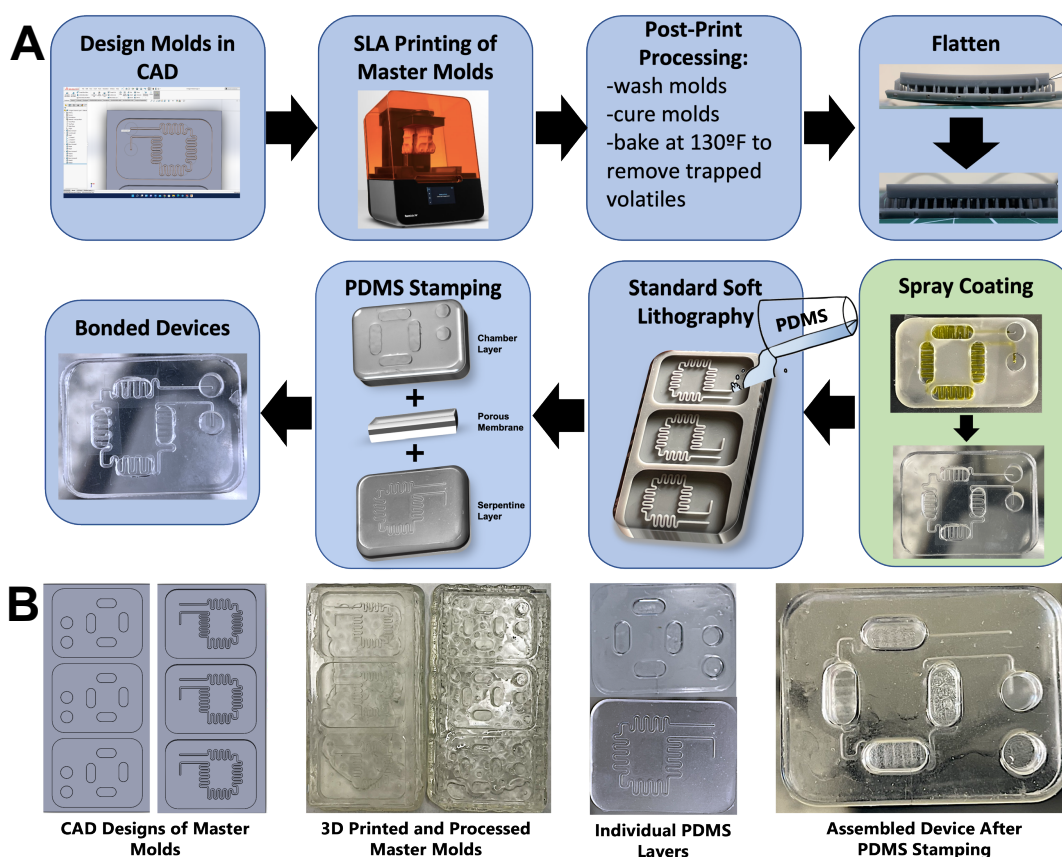


Figure 5: Organ Chip Fabrication Overview A) Digital manufacturing-based workflow enabling rapid prototyping of MPS devices. B) Progression from CAD mold to organ chip

2.11 Device Preparation for Biological Experiments

Prior to cell loading, assembled devices were exposed to ultraviolet light within a cell hood for a minimum of 30 minutes for sterilization. Still under the hood, the devices underwent polydopamine (PDA) treatment to make the surfaces more hydrophilic, a property which promotes gel attachment. The PDA solution comprised of 5 mg/ML of dopamine hydrochloride (Sigma Aldrich) and was injected onto any surface the collagen-fibrin gel would eventually come into contact with. The devices were incubated at room temperature in the dark for roughly 3 hours, then washed a minimum of 2x with sterile

distilled water. Any excess distilled water was aspirated out, and the devices were left to dry overnight.

2.12 Injection Testing

Prior to injecting devices with cell-seeded collagen gels, device iterations were tested using standard food dye. One droplet of coloring was added to a milliliter of water and mixed. The dyed water was then injected into each media channel and gel port to confirm functionality of microfluidic connections within the device. Devices used in this round of testing were discarded after use.

2.13 Cell Culture

Human Umbilical Vein Endothelial cells were cultured in ATTC Vascular Cell Basal Medium supplemented with Endothelial Cell Growth Kit-VEGF and 1% ABAM. Human Lung Fibroblasts were cultured in ATTC Fibroblast Basal Medium supplemented with Fibroblast Grow Kit- Low Serum and 1% ABAM. A549 lung carcinoma epithelial cells were cultured in ATCC F-12K media supplemented with 2% fetal bovine serum, and 1% ABAM. Media was changed every 2nd day. After reaching 80% within a T25 flask, A549 cells were harvested and seeded at 7500 cells/well into an Elplasia spheroid plate. A549 cells were left to form into spheroids for 5 to 7 days before harvesting. HUVECS and A549s were harvested using Corning 0.25% trypsin, while HLFs were harvested using Corning 0.05% trypsin. HUVECS and HLFs were not used past P7. A549s were not used past P10.

2.14 Vasculogenic Gel

HUVECs and HLFs were seeded into collagen-fibrin hydrogels at a concentration of 4M/mL and 2M/mL respectively. For a 1mL aliquot, the hydrogel was prepared as

following: 100 μ L of 10x DMEN, 34.2 μ L of NaOH, 742.6 μ L of Corning Rat Tail Collagen Type I (3.03mg/mL), 125 μ L of 40mg/mL fibrinogen (Sigma-Aldrich), and 8 μ L of thrombin (Sigma-Aldrich) to initiate the conversion of fibrinogen to fibrin. Reagents were kept on ice at all times.

2.15 Device Loading

After hydrogel preparation, devices were immediately loaded. 40 μ L of collagen-fibrin hydrogel was injected into each gel chamber in the membrane device, whereas 30 μ L of collagen-fibrin hydrogel was loaded into each gel chamber for the membrane-free device. For vascular inflammation and spheroid density experiments, A549 spheroids were mixed within the hydrogel and loaded into the first gel chamber only. High spheroid experimental groups were loaded with 1 Elplasia well worth of spheroids (seeded at 7500cells/well) and low spheroid experimental groups were loaded with 0.5 Elplasia wells worth of spheroids (again seeded at 7500cells/well). After gel injection, devices were put in an incubator at 37°C, 5% CO₂, and 21% oxygen for 30 minutes. Devices were briefly taken out to add media. Devices were cultured in static with the above-described VEGF media supplemented with 1% 25mg/mL aprotinin. Devices were left in culture for 7 days and received daily media changes.

2.16 Assessment of Cell Viability

A calcein AM/ethidium-1 live/dead assay (Invitrogen) was used to measure cell viability in the vascularized hydrogels after 7 days in culture. Z-stack images were taken using a Nikon C2 confocal microscope and compressed into a max projection HDR. Images were exported as JPEGs and qualitatively assessed with uniform look-up tables (LUTs).

2.17 Staining and Microscopy

Devices were fixed in 4% paraformaldehyde for 1 hour at room temperature, then overnight at 20°C. After fixation, the hydrogels were removed from the devices and placed in a 48 well plate. Gels were washed and stained with DAPI (Thermo Scientific, Hoescht 33342), Lectin (Vector Laboratories UEA DyeLight 1 594) and ICAM 1 (R&D Systems, BBA3) according to manufacturer protocols. Gels were imaged with a Nikon C2 confocal microscope. Images were taken as Z-stacks comprising of four to six layers with a step size of 4-15 μ m. For use in figures, Z-stacks were compressed into a max intensity HDR file and denoised with the Nikon NIS-Elements software Denoise.ai function. LUTs were adjusted consistently for each individual group of gels imaged.

2.18 Image Analysis

For image analysis, max intensity projection Z-stacks were exported as TIFFs with no LUTs attached. All Image analysis was completed in MATLAB (R2021b). A pretrained deep neural network was used to denoise each image and adaptive histogram equalization was used to standardize contrast across the image set. Vascular network images were then smoothed using an edge preserving filter with a gaussian kernel, and a threshold was applied to remove remaining low-intensity noise. Preprocessed images were then segmented, and morphology was quantified using an open-source automated segmentation tool. All devices stained with ICAM were imaged at a fixed laser intensity, and mean pixel intensity was computed for each image.

2.19 Statistical Analysis

All statistical analysis was conducted in GraphPad Prism 9.2. For membrane-free device gel pinning and detachment rates, a Fisher's exact test was used to calculate the P-value between each pairing of device iterations. For all other statistical analysis, an

unpaired Mann-Whitney test was used. P-values <0.05 were taken to be statistically significant.

Chapter 3: Results

3.1 Multi-Organ Membrane Device V1

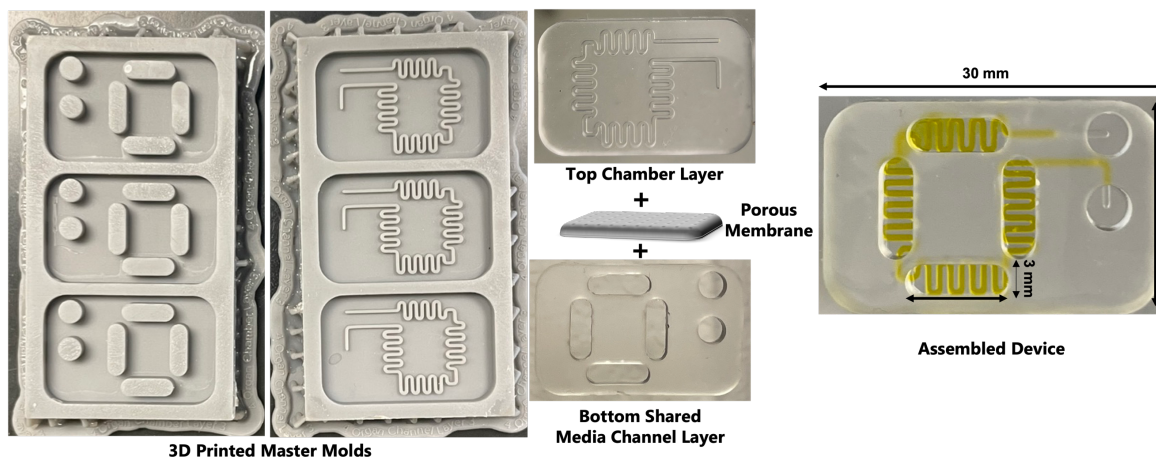


Figure 6: First design iteration of the multi-organ membrane device.

Preliminary testing of V1 for the multi-organ membrane device consisted of injecting food dye into the shared media channel. This was done to assess the functionality of the membranes and the fluidic connections.

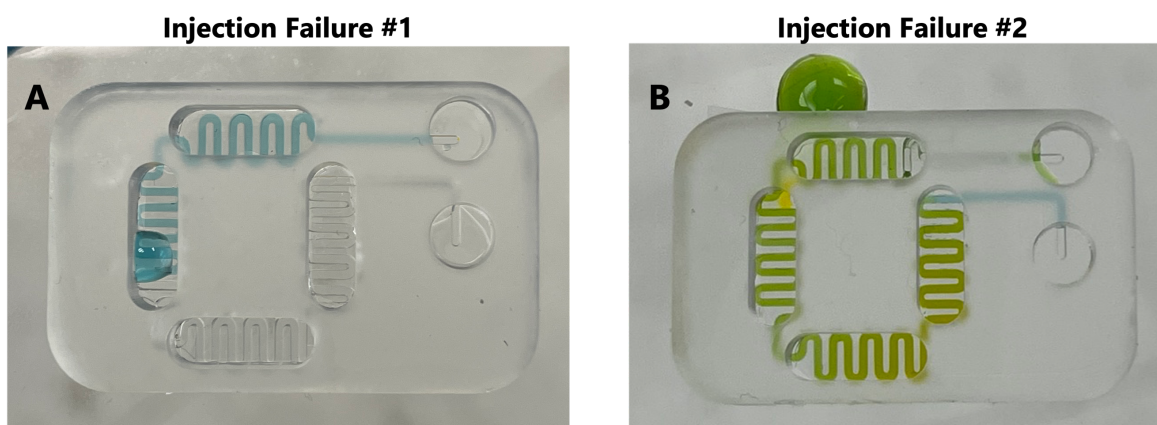


Figure 7: A) Improper coverage of membrane below gel chamber causes media to leak out serpentine channel and into gel chamber. B) Improper bonding of membrane along perimeter of device causes external leakage from serpentine channel.

During testing, two forms of injection failures were observed (**Figure 7**). The first injection failure was leakage of the fluid from the shared media channel into the organ chamber due to improper coverage of the semi-porous membrane. The second injection failure was external leakage of fluid from the shared media channel as a result of improper layer bonding along the edges of the device. V1 of the membrane device had a 0% injection success rate.

3.2 Multi-organ Membrane Device V2

V2 of the membrane device was designed to address the causes of injection failure seen with V1. To avoid leakage of media from the shared channel into the organ chamber, the surface area of the gel chamber in contact with the bottom layer was decreased. The length of the gel chamber was decreased from 9mm to 6.5mm, while the width remained 3mm. The second design change was increasing the distance between device features and the outer perimeter of the device from 1.42mm to 3.55mm. This change allowed for proper bonding of the two PDMS layers to avoid any external leakage. The final design change was to flip the vertical orientation of the media ports of the gel chamber layer. This was done to allow for cloudy surfaces (face cured against the mold) of each PDMS layer to be bonded together. Bonding the cloudy PDMS faces together mimics the effect of spray coating by improving device transparency. Injection testing of 43 membrane device V2 resulted in a 100% success rate. With such a high success rate, we moved forward with using V2 for biological experiments.

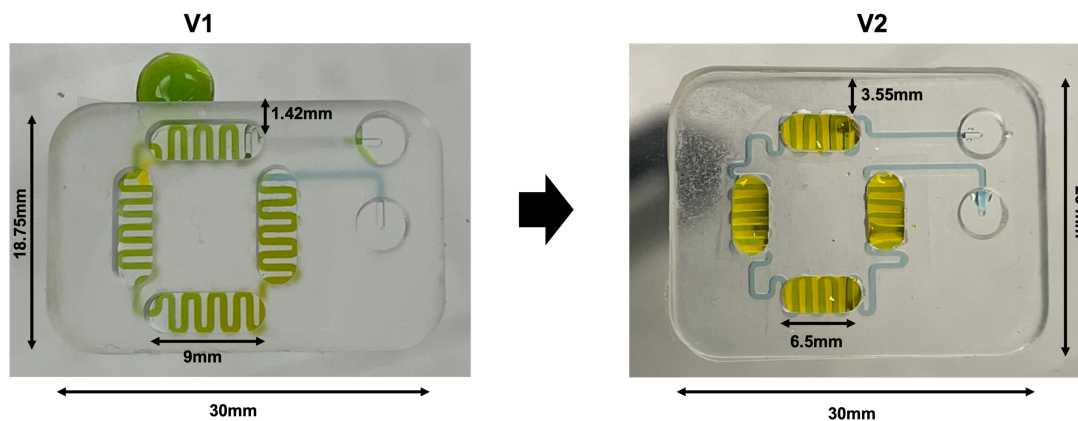


Figure 8: Design Changes Between Iteration 1 and Iteration 2 of multi-organ membrane device.

The next round of testing V2 membrane devices involved culturing vasculogenic hydrogels as previously described in all four “organ” chambers. A549 spheroids were suspended in the vasculogenic hydrogel and injected into the “cancer” chamber. Chambers 1 through 3 were loaded only with the vasculogenic hydrogel. They were left in culture for 7 days before being fixed and stained to assess vascular network formation.

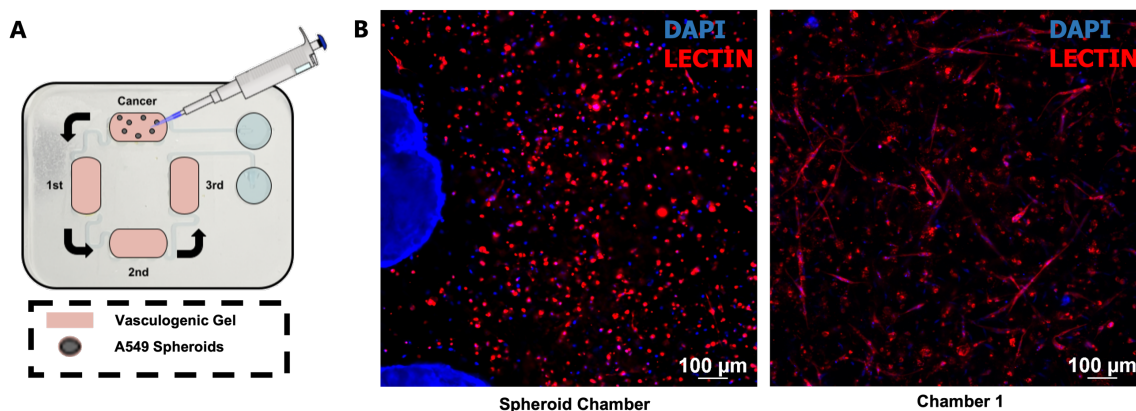


Figure 9: Assessment of Vascular Formation in V2 Membrane Devices (A) Injection of V2 membrane device with A549 spheroids and vasculogenic collagen-fibrin hydrogel containing 4M/mL HUVEC and 2M/mL HLF. (B) DAPI and

Lectin staining of hydrogels after 7 days in culture for qualitative assessment of vessel formation.

DAPI and Lectin imaging showed minimal to no vascularization within the V2 collagen-fibrin hydrogels. By Day 7, it is expected for a well-established vascular network to have formed. This hinted to an issue with cell viability, which was addressed by assessing media consumption.

3.3 V2 Media Consumption Calculations:

For HUVECS and HLFs cocultured in a hydrogel at 6M/mL seeding density, the accepted consumption rate of media over a 24-hour period is $10\mu\text{L}$ per $1\mu\text{L}$ of gel.¹¹ Each device has 4 chambers, and each chamber is injected with $40\mu\text{L}$ of hydrogel. So, each device holds $160\mu\text{L}$ of gel and will presumably consume $1600\mu\text{L}$ of media over 24 hours.

To calculate how much media one device holds, I added up the volumes of each of the media-containing compartments. It was found that the V2 device could hold a maximum of $573\mu\text{L}$ of media. This means that in order for the cells to be sustained in culture, they would need a media change every 8.6 hours. Media was only being changed every 24 hours. This variance in media renewal almost certainly accounted for the lack of cell viability after 7 days in culture.

3.4 Multi-organ Membrane Device V3

Having to change media three times a day on a device is unrealistic and significantly decreases the usability a device. For the third iteration of the multi-organ membrane device, this issue was addressed by increasing the volume of media each device could hold. The holding volume of media was increased by changing the chamber layer depth from 3mm to 4mm, and by adding a second, identical chamber

layer to every fabricated device. This 5mm increase in height decreased the media renewal requirement to once every 16.5 hours.

V3 of the membrane device was tested by again culturing a vasculogenic hydrogel in each of the 4 organ compartments, with A549 spheroid in the first chamber. At day 7, devices were either stained for lectin to assess vessel formation or with a live/dead to assess cell viability.

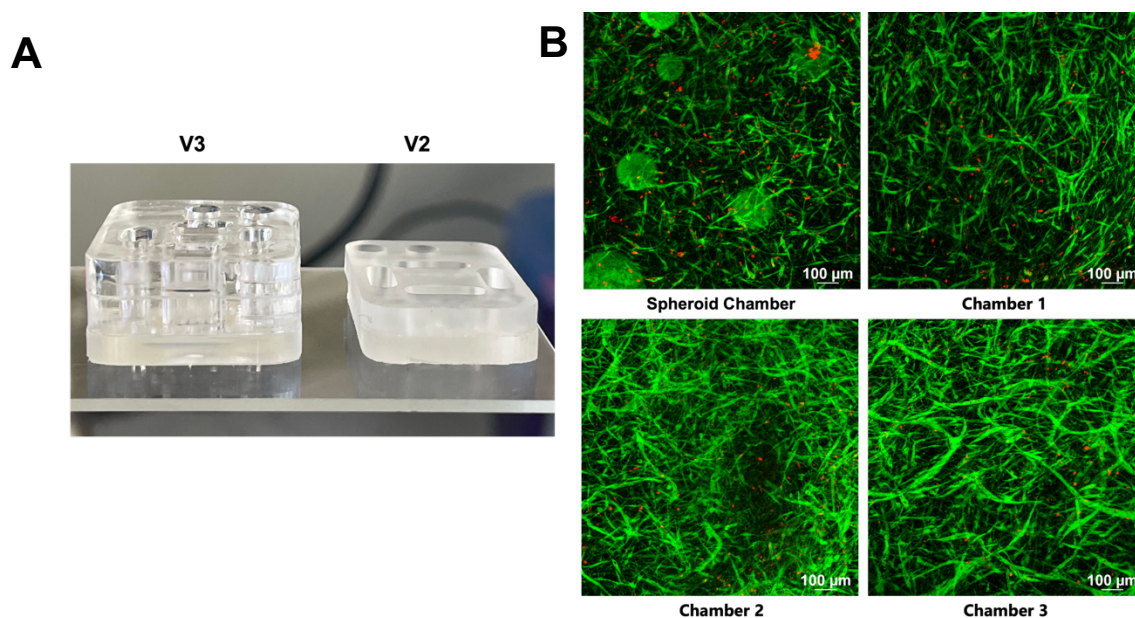


Figure 10: Assessment of Cell Viability in V3 membrane device. A) Design changes between V2 and V3 of the membrane device. B) Live/dead staining for assessment of cell viability after 7 days in culture. Calcein AM stain corresponds to live cells (green), while Ethidium-1 corresponds to dead cells (red).

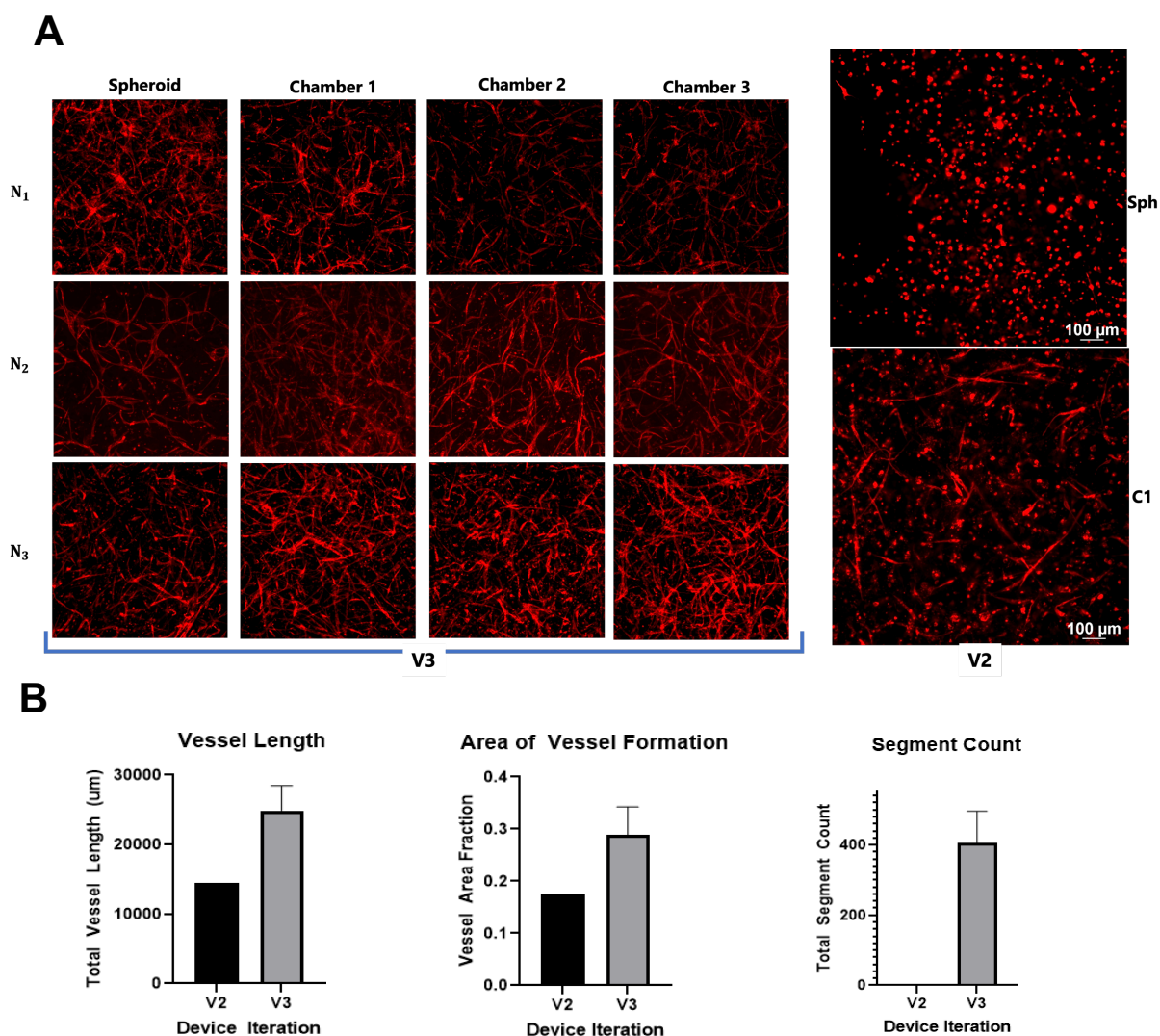


Figure 11: Quantification of Vessel formation in V2 and V3 membrane device hydrogels. A) Lectin staining of vascularized hydrogels after 7 days in culture. B) Morphological assessment of V2 versus V3 in terms of vessel length, area of vessel formation, and segment count.

Results from the live/dead assay in **Figure 11** show a substantial increase in cell viability and vessel formation from V2 to V3 of the multi-organ membrane device. This was qualitatively assessed by observing the overwhelming green signal compared to the red. Images stained with Lectin (**Figure 11**) also show vascular formation through the organization of HUVECS into tubular structures. A morphological analysis of the

vascular network found a substantial increase in vessel length, area of vessel formation, and segment count from V2 to V3.

The final experiment with V3 membrane devices serves to validate the crosstalk between chamber compartments. Vascular inflammation was used as a measure of this inter-organ communication given its role in promoting tumor progression and metastasis. Vascular inflammation was quantified by measuring ICAM-1 expression. The hypothesis for this experiment was that ICAM-1 expression would be evident across all four organ chambers. After culturing spheroids and HUVECs/HLFs in collagen/fibrin hydrogel, devices were fixed after 7 days. Gels were removed from the device and stained for DAPI, Lectin, and ICAM-1.

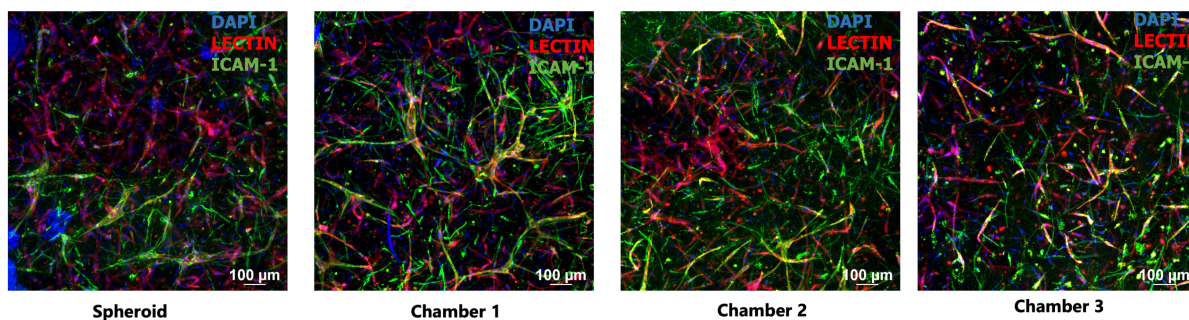


Figure 12: DAPI, Lectin, and ICAM-1 staining for assessment of vascular inflammation.

As shown in Figure 12, ICAM-1 expression is evident across all four organ chambers. The overlap of ICAM-1 signal with lectin indicates there indeed was vascular inflammation induced in each organ chamber. Notably, there is also ICAM-1 being strongly expressed by the fibroblasts, suggesting the cancer signals are inducing some sort of stress on the fibroblasts.

3.5 Multi-organ Membrane Free Device

My work involving the multi-organ membrane-free device consisted of two major components: optimizing the workflow of fabricating membrane-free devices and optimizing the device itself. For optimization of the fabrication workflow, my main focus was on reducing fabrication time by moving away from replica molding, analyzing the efficiency of spray coating, and improving the PDA treatment protocol. The parameters chosen to analyze success of the membrane-free devices included gel pinning rate, gel anchorage, validation of vascular network formation, and validation of crosstalk between organ chambers.

3.6 Moving Away from Replica Molding

As discussed earlier, replica molding is a technique under the umbrella of soft lithography in which 3D printed master molds are used to make PDMS replica molds, which are then used to pour PDMS organ chip layers. In our situation, replica molding was initially used to overcome 3D printing limitations of negative features on the milli-scale. However, there are certain aspects of replica molding that make it an unfavorable fabrication technique. Firstly, replica molding requires an additional stage of PDMS pouring. This can add up to two days to a device's fabrication time depending on whether or not the PDMS is cured at room temperature. In addition, replica molds are extremely fragile. They are prone to tearing and easily deform after a just a few uses. Another limitation of replica molding is the increased likelihood of feature distortion. Anytime a mold is poured, there will be a small tolerance in the dimensions of the patterned features on the poured layer.²⁸. Replica molding involves two pourings, so the chance of feature distortion is increased.

To move away from replica molding, the plane in which the chambers are divided was changed. In a replica molded device, the bottom PDMS layer only contains the

guide structures. However, in the non-replica molded devices, the bottom and middle layer molds are split directly across the center of the channel heights. Design iterations 1 through 4 of the multi-organ membrane-free device have moved away from use replica molding.

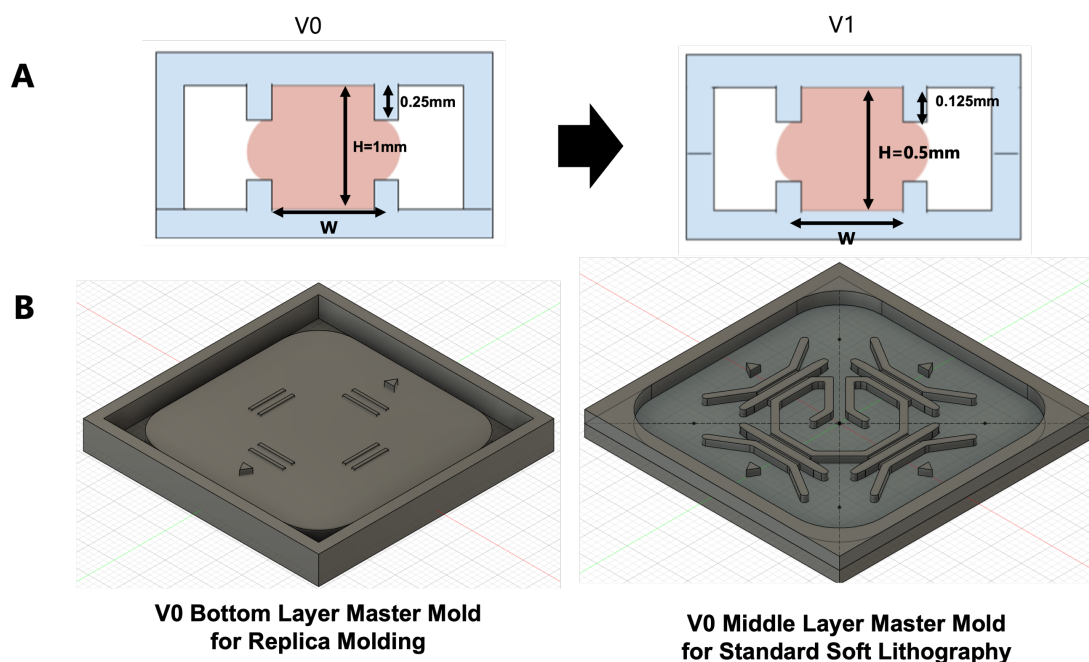


Figure 13: Membrane-Free Components A) Cross-sectional view of switching away from replica molding. B) Middle and bottom octagon chip layers associated with V0 replica molding.

3.7 The Effects of Spray Coating

To address surface imperfections that make PDMS appear opaque after curing, 3D printed molds in our lab are normally sprayed with a thin layer of automotive clear coat. This clear coat is applied by hand using an airbrush. Clear coating molds before pouring them improves transparency of PDMS layers which minimizes optical interference for in-device imaging. Spray coating also adds a protective layer to your

mold to avoid surface scratching. However, there are some drawbacks to spray coating associated with our non-standardized method of application.

Our hand-held method of spray coating introduces inconsistencies that can affect device success. To begin, it is difficult to get a perfectly even distribution of the spray coat. Uneven distribution causing a bubbling effect in which clumps of clear coat randomly accumulate on the surface. These clumps can cause issues with bonding PDMS layers together. Also, if the bubbling is near significant features, there could be distortion and loss of function. Furthermore, there is a thin margin for which surface imperfections are erased without the spray coating layer being too thick. If a spray coating layer is too thick, it can cause the features to distort. If a spray coating layer is too thin, then optical clarity will not be met.

These studies revealed that membrane-free devices are particularly sensitive to feature distortion caused by clear coating. When the geometry of guide structures is altered, this reduces surface tension and can lead to device failure via the pooling over of gel into adjacent channels. My device having four membrane-free interfaces on 2 different axes increases the difficulty of achieving an even distribution. Later experiments incorporated devices from non-spray coated molds, which enabled more consistent and successful loading of gels.

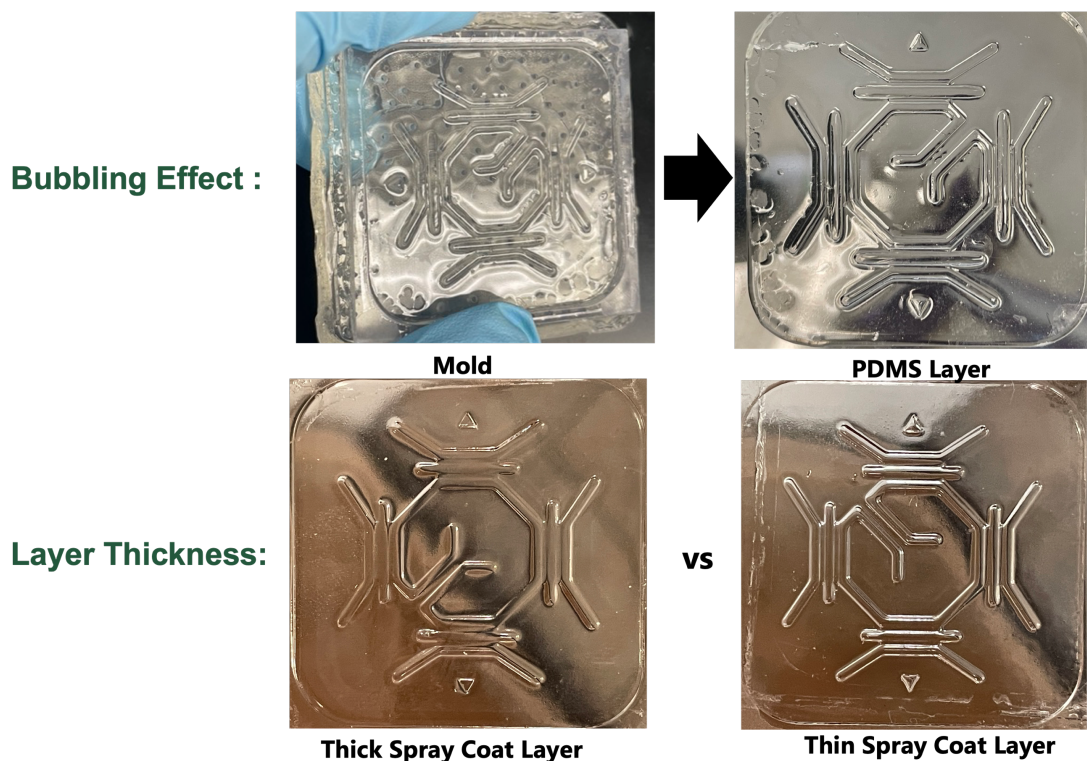


Figure 14: Feature Distortions Caused by Clear Coating

3.8 Improving Gel Anchorage

Another component of the fabrication workflow I optimized for my multi-organ membrane free devices was the PDA treatment protocol. PDA is a surface treatment that reduces the likelihood of gels detaching from the PDMS or membrane surface. PDA treatment works by promoting the binding of ECM proteins to the PDA layer on the PDMS. A multi-faceted approach was taken to improve gel attachment over the course of device culture. For one, the PDA protocol was adjusted to increase the incubation period of PDA treatment from 2 to 3 hours and increase concentration from 2mg/mL to 5mg/mL. Another approach was to stop spray coating my molds to improve surface roughness of the gel chamber. Small surface imperfections on the PDMS give the gel more to anchor to and overall improve gel attachment. The final approach taken to

improve gel attachment was adjusting the device itself. For V4 of the membrane-free device, I increased the inlets of the gel chamber from 1 to 1.5mm. This increase in surface area provided more space for the gel to attach to.

Two means of gel detachment were observed over the course of various device loadings (**Figure 15**). First, there was a buckling effect in which the end of the gel completely released from the PDMS and contracted inwards. This form of gel detachment was severe and affected the functionality of the fluidic system. The second means of gel detachment was a necking effect, in which the gel was starting to release from the sides but has not fully contracted inwards. Less severe gel detachment such as the necking effect would often progress to complete detachment of a gel in a matter of days.

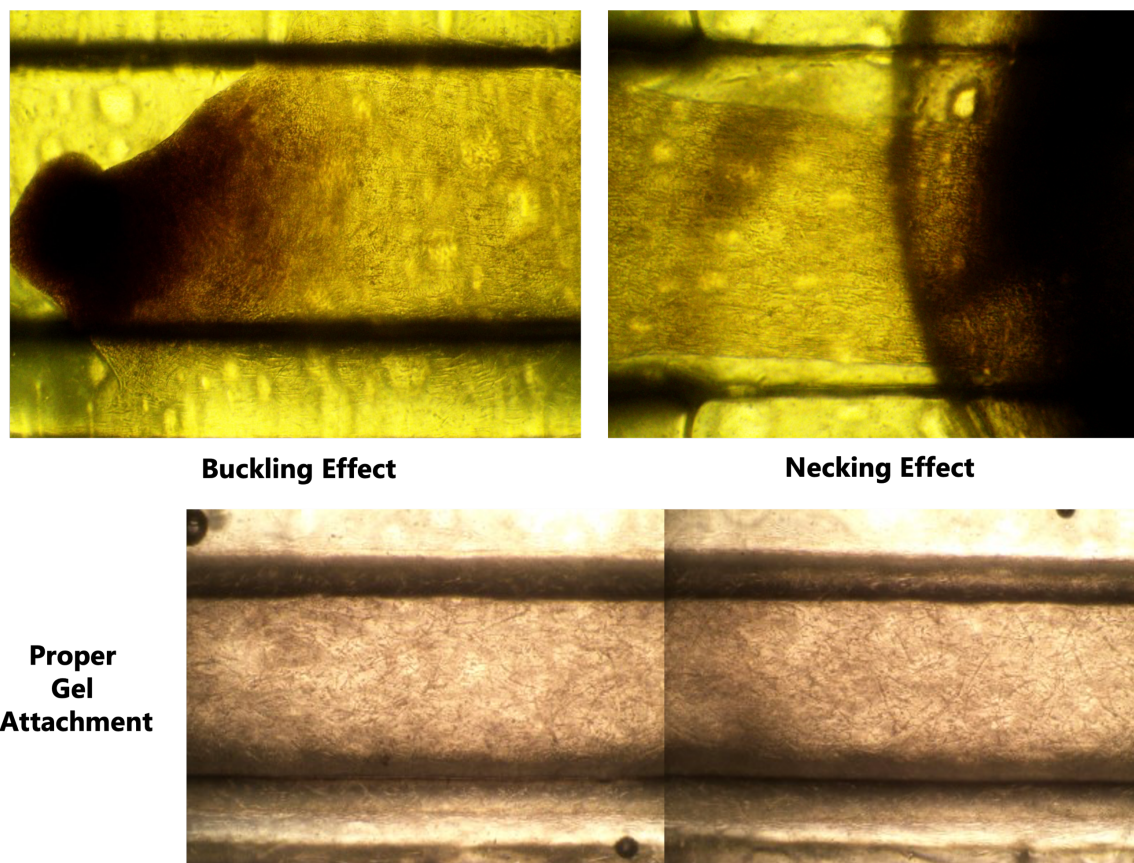


Figure 15: Means of Gel Detachment

3.9 Membrane- Free Device Iterations

The initial parameters used to determine device success were gel pinning rates and gel detachment rates. Device iterations were rapidly fabricated and tested based on these two parameters. Other factors were also considered, such as moving away from replica molding as we see in the transition from V0 to V1. Below are the various design iterations and the outcomes from testing.

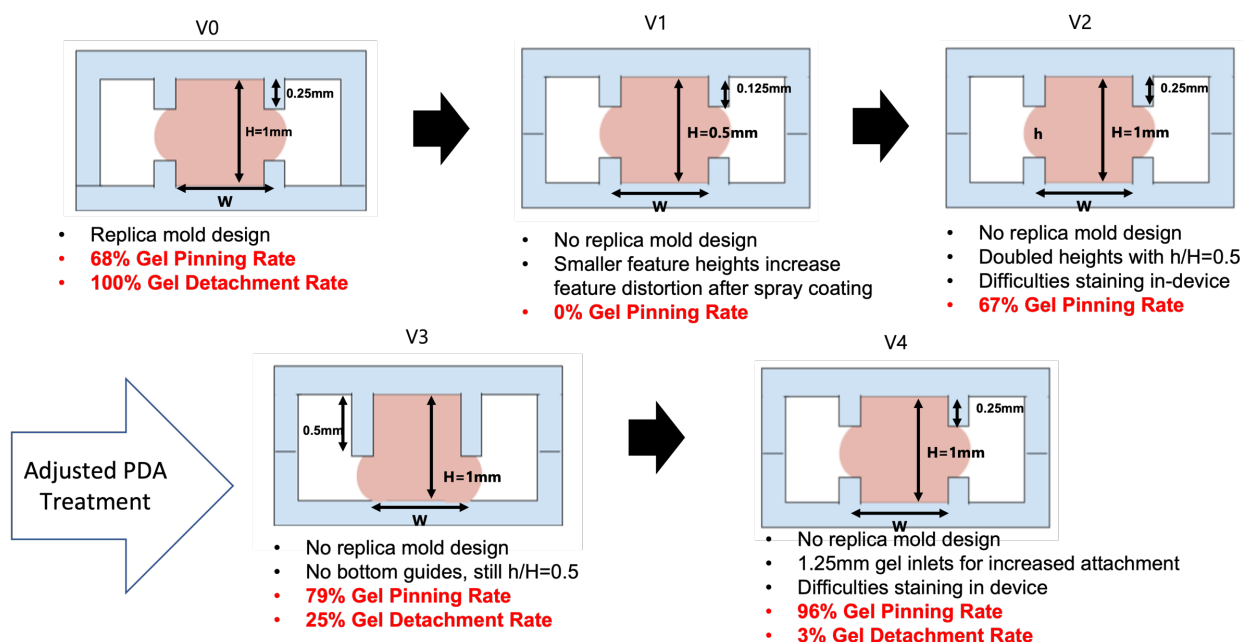


Figure 16: Design Iterations for Multi-Organ Membrane-Free Devices.

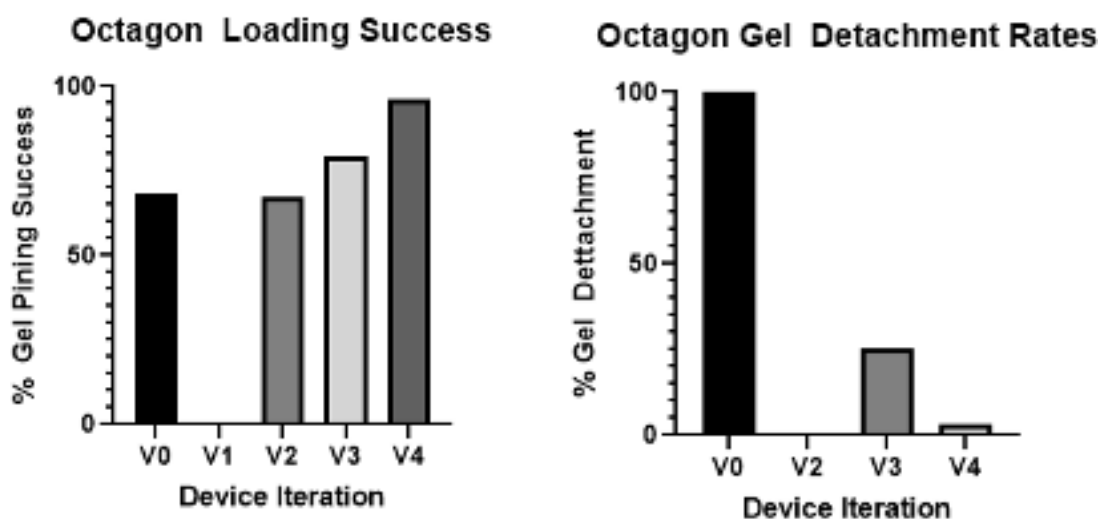


Figure 17: Gel Pinning and Detachment Rates Vary by Device Iteration

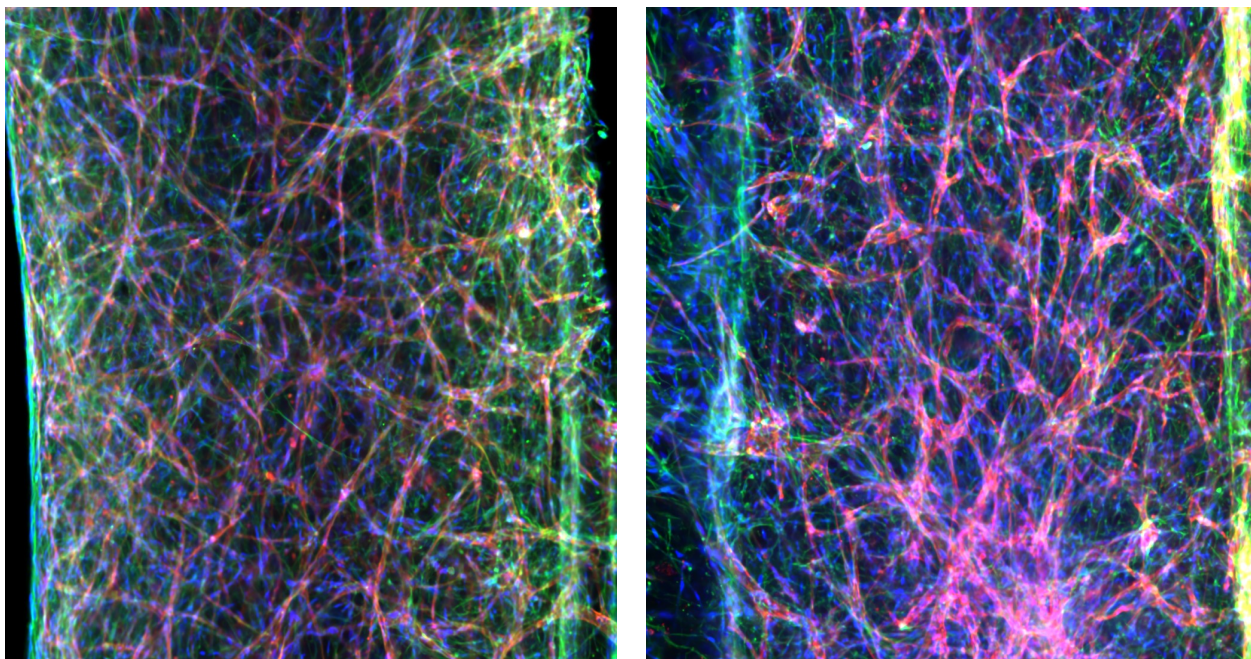
As stated previously, the biggest change between membrane-free V0 and V1 was moving away from replica molding. The replica molded devices were not only time consuming to fabricate, but also had relatively low rates of loading success and poor gel detachment. V1 decreased the overall heights of the device channels and guide structures while keeping $h/H=0.5$. This was done in an attempt to conserve materials; however, the shortened features were so easily distorted by spray coating that this iteration had a 0% gel loading rate. V2 went back to the original channel and guide heights seen with V0. There was minimal difference between the loading rates of V0 and V2. This finding makes sense as the end design is the same. With V2 of the devices, there were difficulties in getting the stains to fully penetrate the gel within the device. To address this staining issue, in V3 I removed the bottom guide structures and doubled the height of the top guide structures to maintain $h/H=0.5$. This resulted in the bottom layer becoming a plain slab of PDMS with alignment features. V3 had a decent increase in gel pinning rate going from 67% to 79%, however, gel detachment was high at 25%. The final design iteration went back to the V3 configuration but with increased inlet size of the

gel chambers to increase gel attachment. This iteration has been most successful thus far in terms of both gel loading rates and gel detachment. V4 of the membrane-free device had a 96% gel pinning rate and only 3% gel detachment. There was a significant increase in loading success of V4 compared to V3, V1, and V0. A Fisher's exact test was used to determine a P-value of 0.0001 between V0 and V4 (**Table 1**). V4 and V3's were used for the following experiments.

	Calculated P-value	Significant?
V0 vs. V1	<0.0001	Yes
V0 vs. V2	>0.9999	No
V2 vs. V3	0.6067	No
V3 vs. V4	0.0025	Yes
V0 vs. V4	<0.0001	Yes

Table #1: Contingency Data Analysis of Membrane-free device gel pinning rates using Fisher's exact test.

The next round of testing involved the validation of vascular network formation within the gel compartments. Again, devices were seeding with vasculogenic collagen-fibrin hydrogels. After 7 days in culture, devices were stained, and gels were taken out for imaging.



Gel Chamber 1

Gel Chamber 2

Figure 18: Assessment of vascular formation in vascularized gels. Gels were fixed at Day 7 and stained with DAPI, Lectin, and Phalloidin

The images from **Figure 18** exhibit a well-established network by day 7. Almost all present cells are participating within the vascular network. There is even some evidence of anastomosis.

The next step was to validate crosstalk between the organ compartments by looking at ICAM-1 expression. A549 spheroids were placed in the cancer chamber within each device, while the other three chambers contained only the vasculogenic hydrogel. Devices were fixed at Day 7 and stained for DAPI, Lectin, and ICAM-1. The hypothesis for this experiment was that the ICAM-1 signal would be evident across all 4 chambers, with signal intensity increasing in the presence of spheroids. Another hypothesis was that ICAM-1 signal would decrease with distance from the spheroid chamber.

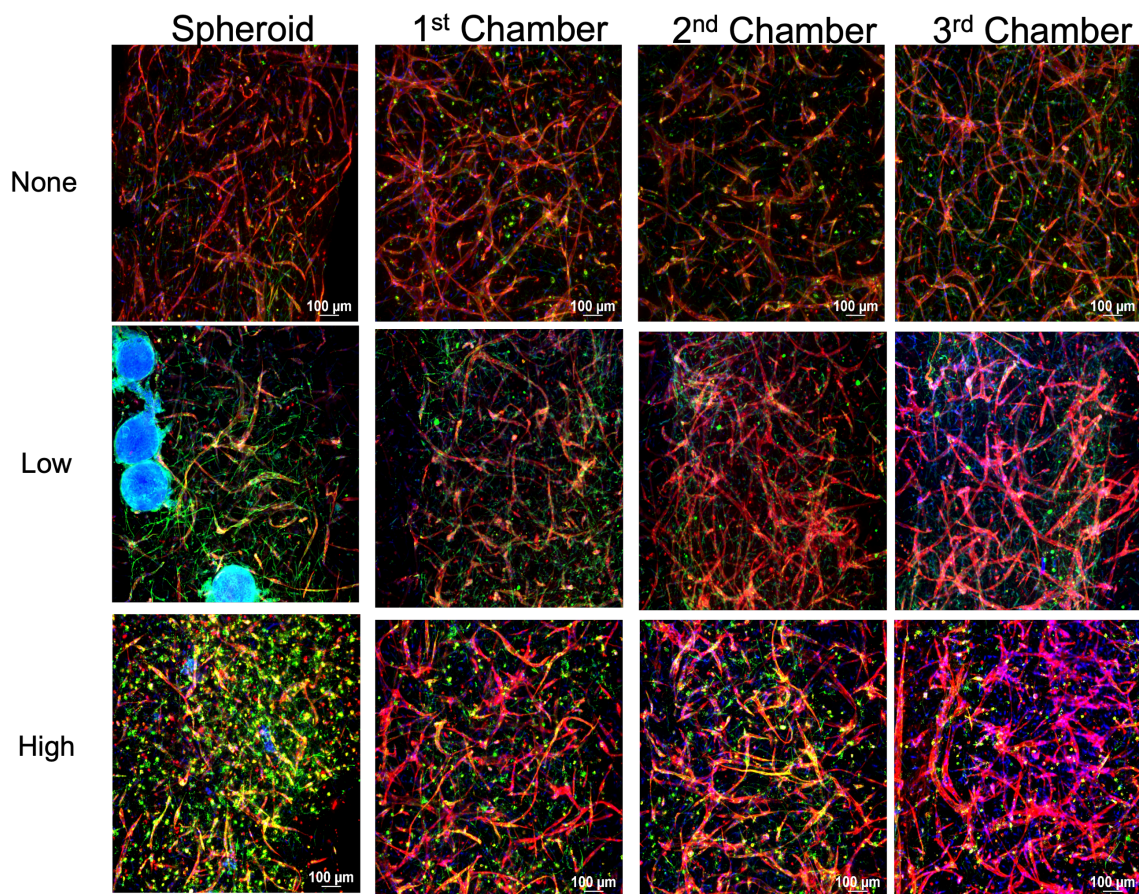


Figure 19: DAPI, Lectin, and ICAM-1 staining of vascularized hydrogels at Day 7 in culture. The cancer chamber of each device was filled with no, low, or a high count of spheroids.

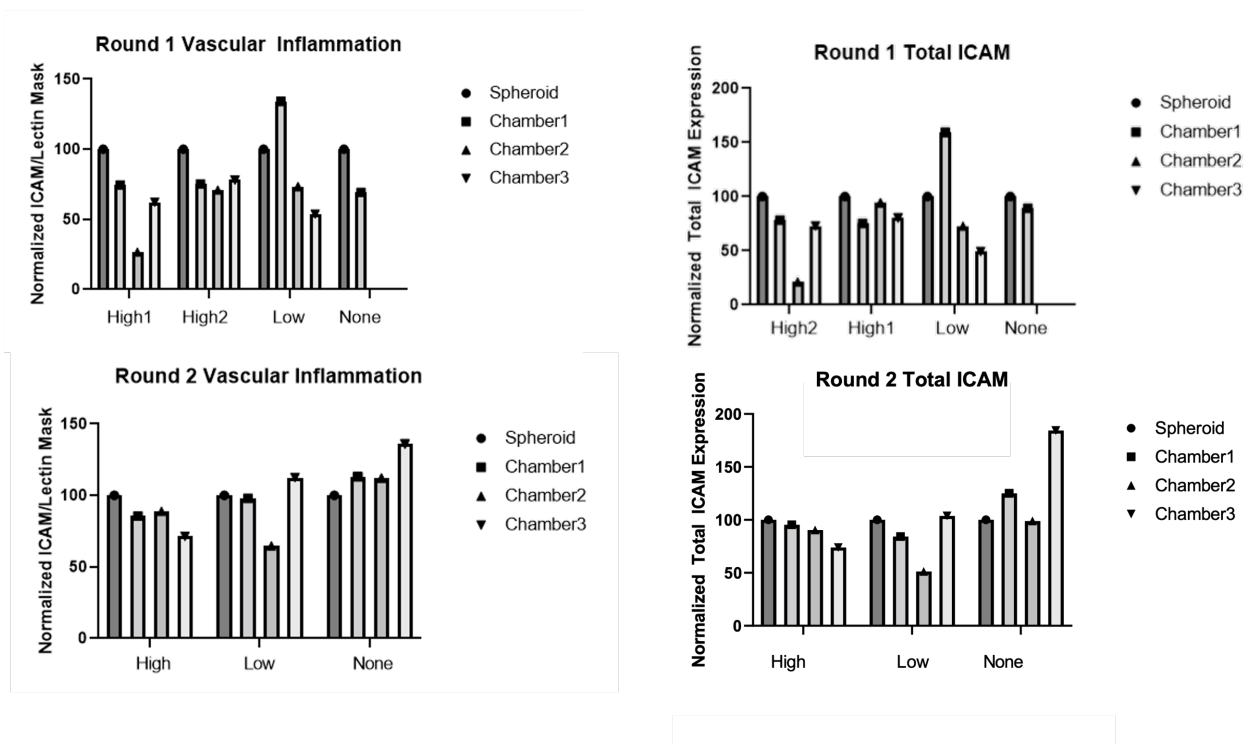


Figure 20: Quantification of ICAM-1 Intensity Across Chambers. ICAM-1 Expression was measured and normalized to the spheroid compartment within each device.

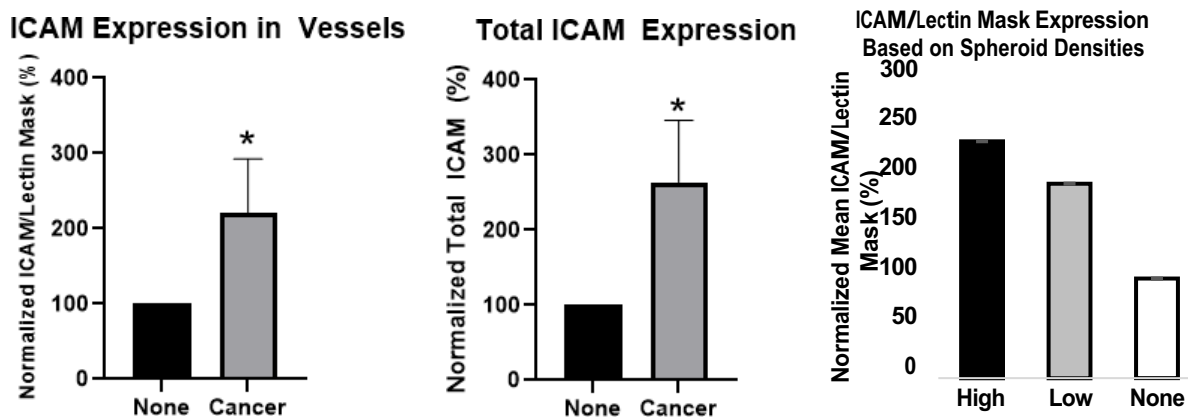


Figure 21: Variations in ICAM-1 Expression Between Cancer and Control Groups. Mean ICAM-1 Expression was measured and normalized to the control group.

Two measures of ICAM expression were quantified using MATLAB for image analysis. The first was the mean total ICAM-1 expression found within each image. The

second measurement was the mean masked ICAM/Lectin expression. The overlap between ICAM and Lectin signal is indicative of there being vascular inflammation within the vascular gels.

Looking at **Figures 19-21**, we see vascular inflammation across all organ chambers. With the exception of one device, there was a trend of ICAM-1 expression being highest in the spheroid compartment of each device. However, no conclusive trend was observed in the variations of ICAM-1 expression between non-cancer chambers in each device. There was no significant difference in ICAM-1 expression between high and low spheroid density groups. However, after pooling the high and low spheroid density groups and normalizing to the control, we see a significant change in ICAM-1 expression for devices with spheroids. This significant difference was observed in both the total ICAM expression and with the ICAM/lectin mask. This result validates that signals from the cancer cells are in fact eliciting effects on the cells in the other organ chambers.

Chapter 4: Discussion and Conclusion

Two separate microphysiological platforms were developed to model the effects of a pathology across multiple organ constructs. The primary functions of these models were to sustain the culture of multiple tissues while facilitating transport and communication between them. A particular emphasis was placed on enabling physiologically relevant transport through the development of a vascular network within the tissue constructs. The first device incorporated the use of membranes and vertically stacked compartments to enable bulk vascularization of 3D tissue within each of the chamber compartments. The second device progressed one step closer to having a functional vascular network through the incorporation of open interfaces to allow for the free transit of cells between compartments. This was accomplished using membrane-free technology driven by surface tension. A digital manufacturing-based fabrication workflow was used for rapid prototyping of organ chip devices. Devices were iteratively designed and optimized to have a high success rate for hydrogel loading and maintaining gel adherence when in culture. Both modeling platforms were then used in biological experiments to explore how tumor signals in one compartment elicit effects on the other tissue constructs.

Three different versions of the multi-organ membrane model and five different versions of the multi-organ membrane-free model were designed and tested over the course of this thesis. The final iteration of the membrane device, V3, increased the loading rate from 0% with V0 to 100%. Cell viability after 7 days in culture was also drastically improved by increasing the volume of the media compartments. Iterations of the membrane-free device improved initial gel loading rates from 67% to 96%. Gel detachment was improved from 100% to only 3% by adjusting the design of the device in addition to optimizing the polydopamine treatment protocol.

4.1 Digital Manufacturing-Based Organ Chip Fabrication

Rapid iterating and testing of device designs would not have been possible without the 3D-printing based fabrication workflow developed in our lab. However, there are certain limitations of this workflow for fabricating organ-chip devices that must be addressed. For one, the FormLab 3D printer is limited in resolution on the micro-scale. Previous experiments in our lab have found that the printer can only correctly pattern positive channels as small as $200\mu\text{m}$ and negative channels as small as $400\mu\text{m}$.²⁵ This constricts the size of features we are able to incorporate into our organ chips.

Because patterned features necessary for organ chip systems are on the micro and milli-scale, organ chip molds are extremely sensitive to feature distortion. This is most evident in the fabrication step of clear coating the molds. Clear coating is necessary to smoothen micro-imperfections on the surface of the 3D printed molds. Our lab only has the capability to clear coat molds using a handheld airbrush which makes standardization and getting an even distribution of the clear coat difficult. Random bubbles would often form on the surface of the mold leading to issues with bonding device layers together. If the bubbling was situated near patterned channels or other important features, this would make the mold unusable. Spraying too thick of a clear coat layer would often lead to feature distortions that drastically reduced gel pinning rates. This was especially evident with the membrane-free devices in which maintaining guide structure and channel geometry is essential for creating the necessary the surface tension. Spray coating difficulties were exacerbated by the complexity of the features with the multi-organ membrane-free device. The gel chambers and associated membrane-free technology are not only tightly packed, but they are also oriented along two different axes. This makes it extremely difficult to avoid over-spraying features

perpendicular to the path of your spray coating strokes. For each new membrane-free design, it would take roughly two or three attempts at spray coating before I got a functional mold. For the reason, certain molds for later experiments were no longer spray coated. This protocol change was based on the fact my experiments did not require me to keep the gels in the device from staining and imaging. Not spray coating brought more consistency to the loading rates of my devices. V4 of the membrane-free devices maintained high gel injection rates when not spray coated. However, the no-bottom guide design (V3) consistently performed poorly when not spray coated.

4.2 Design Constraints of Membrane Devices for Media Consumption

Functional versions of the membrane and membrane-free device platforms were seeded with vasculogenic hydrogels as “placeholders” for multiple organ types. A549 spheroids were loaded only in the cancer chamber to study how the tumor signals affected the other compartments. Lectin staining of the vasculogenic hydrogels of V2 membrane devices revealed little to no network formation. The cells were also extremely rounded which implies the cells were under extreme duress and probably did not survive the week in culture. Media consumption was believed to be the culprit of having low cell viability. This hypothesis was formulated based on the media being a bright yellow when daily media changes were performed. The V2 membrane design required media to be replaced every 8 hours. The volume of media reservoirs was increased with V3 to require less frequent media changes of once every 16.5 hours. Media renewal requirements of every 24-48 hours are ideal, however, achieving that was not possible with this device. One constraint is that the area of the gel chamber opening could not be increased without affecting the functionality of the membrane/serpentine channel interface. The other constraint is that the depth of the chamber layer could not be increased passed 4mm because cured PDMS layers tend to get stuck in the master molds the thicker you make them.

4.3 Vascular formation in Organ Compartments

Assessment of vascularization in the various organ compartments revealed some interesting trends. For both membrane and membrane free devices, chambers loaded with A549s had less network formation than the non-cancer compartments. Spheroid chambers also had higher rates of ICAM-1 expression and vascular inflammation. This finding is fascinating being that inflammation is known to promote angiogenesis in both in vivo and in vitro settings. One reason blood vessels are forming at a lower rate may have to do with the metabolic intake of the tumor. It is possible the tumor is taking nutrients away from the endothelial cells and causing them to die or undergo phenotypic changes. Another possibility is that the tumor is releasing chemical signals inhibiting angiogenesis.

4.4 Vascular Inflammation and ICAM-1 Expression

Another observation was that there was no significant difference in ICAM-1 expression for devices loaded with a high density of spheroids versus a low density of spheroids. One reason this could be the case is that a better mechanism of harvesting spheroids is needed. A549 cells are seeded at the same density in Elplasia spheroid wells and cultured for 5 to 10 days. Each well contains 96 micro-compartments that encourage spheroid formation. For high density spheroid loadings, one Elplasia spheroid well was harvested. For low density spheroid loadings, one half of an Elplasia spheroid well was harvested. The issue comes in that it is impossible to guarantee that you have collected all of the individual spheroids within each well. The inconsistencies in the number of spheroids harvested from each well may require there to be a greater disparity between high and low groups for distinct spheroid densities to actually be achieved.

One hypothesis I had for the ICAM-1 experiments was that ICAM-1 expression would decrease with increasing distance from the spheroid compartment. This

hypothesis was partially supported by the fact that in most devices, the spheroid chamber had the highest rate of ICAM-1 intensity. However, there was no significant difference in ICAM-1 between chambers 1, 2, and 3. If anything, an opposite trend was starting to emerge with chamber 3 expressing more ICAM-1 than chambers 1 and 2 for two of the octagon devices. More repetitions of this experiment need to be done before any solid conclusions can be made.

An explanation for why a difference in ICAM-1 between chambers 1, 2, and 3 was not observed could have to do with the method of culture. All devices were cultured in static for a period of 7 days. This lack of constant flow could have minimized gradient production of ICAM-1 signals and caused the three chambers to somewhat balance out. Incorporation of flow through either a pump or orbital rocker would better replicate physiological conditions.

For V3 of the membrane device, a preliminary experiment found there to be ICAM-1 expression in all four gel chambers. Some degree of vascular inflammation was also observed based on the overlay of the green signal ICAM signal with the red lectin signal. This experiment showed there was in fact communication between the different tissue constructs. However, time constraints did not allow for enough repetitions to be ran for any further conclusions to be made.

4.5 Conclusions and Future Work

Two separate microphysiological modeling platforms were developed to study intercellular communication between multiple tissue chambers in a single, interconnected system. Both models incorporated 3D vascularized tissue constructs, with the second model enabling cell transit between compartments necessary for various organ-level processes, including vascular invasion and anastomosis. The sustainability of these devices to culture multiple tissue constructs was validated with live/dead assays and morphological

analysis of vascular network formation after 7 days in static culture. Further, communication between the various compartments was validated by measuring vascular inflammation induced by A549 spheroids in one of the organ compartments. Devices were optimized to have a 100% and 96% gel injection rate. The membrane-free device was further optimized to have a gel detachment rate of only 3% (compared to the 100% detachment rate seen with the initial design iteration). Ultimately, ease of use was achieved across both modeling platforms.

Given such an early stage in development of these models, there are a multitude of paths this project could continue along. The first is building up to having a fully functional and perfusable vascular network to facilitate transport between the multiple organ constructs. This could be accomplished by seeding side channels with endothelial cells to promote anastomosis and incorporation of a peristaltic pump for vascular maturation. Other projects in our lab are currently working to accomplish this with a single chamber membrane-free organ chip.

A long-term goal for our lab is to eventually use these models to study the complex interactions of energy-wasting processes associated with cancer-induced cachexia. This would require the incorporation of various organ constructs such as liver, muscle, and fat tissue. The muscle and fat tissue would be investigated for degradation and endocrine changes, while the liver would be looked at for metabolic cycle changes such as the switch to the Cori cycle and gluconeogenesis. The hope is to also optimize each individual organ compartments to mimic biological structure and function. Previous work by Dr. Mondrinos has already developed an anisotropic musculoskeletal organ construct and looked at the effects of cachexia.³⁰ These modeling platforms would build upon that work through the incorporation of a variety of organ types. Systemic

inflammation is known to play a role in cachexia, so having a fully vascularized organ chip would further improve physiological relevance.

Further future work with both models could include looking at absorption, distribution, metabolism, and excretion processes for assessing drug toxicity.

List of References

1. Hu, Q., Hao, C., & Tang, S. (2020). From sepsis to acute respiratory distress syndrome (ARDS): emerging preventive strategies based on molecular and genetic researches. *Bioscience Reports*, 40(5). <https://doi.org/10.1042/bsr20200830>
2. Cooper, G. (2018). *The Cell: A Molecular Approach* (8th ed.). Sinauer Associates is an imprint of Oxford University Press.
3. Tumor microenvironment: the promising target for tumor therapy. (2014). *Cancer Cell & Microenvironment*. <https://doi.org/10.14800/ccm.81>
4. McDowell, S. A. C., & Quail, D. F. (2019). Immunological Regulation of Vascular Inflammation During Cancer Metastasis. *Frontiers in Immunology*, 10. <https://doi.org/10.3389/fimmu.2019.01984>
5. Narsale, A. A., Enos, R. T., Puppa, M. J., Chatterjee, S., Murphy, E. A., Fayad, R., Pena, M. O., Durstine, J. L., & Carson, J. A. (2015). Liver Inflammation and Metabolic Signaling in ApcMin/+ Mice: The Role of Cachexia Progression. *PLOS ONE*, 10(3), e0119888. <https://doi.org/10.1371/journal.pone.0119888>
6. Rohm, M., Zeigerer, A., Machado, J., & Herzig, S. (2019). Energy metabolism in cachexia. *EMBO Reports*, 20(4). <https://doi.org/10.15252/embr.201847258>
7. Duval, K., Grover, H., Han, L. H., Mou, Y., Pegoraro, A. F., Fredberg, J., & Chen, Z. (2017). Modeling Physiological Events in 2D vs. 3D Cell Culture. *Physiology*, 32(4), 266–277. <https://doi.org/10.1152/physiol.00036.2016>
8. Horman, S. R., To, J., Lamb, J., Zoll, J. H., Leonetti, N., Tu, B., Moran, R., Newlin, R., Walker, J. R., & Orth, A. P. (2017). Functional profiling of microtumors to identify cancer associated fibroblast-derived drug targets. *Oncotarget*, 8(59), 99913–99930. <https://doi.org/10.18632/oncotarget.21915>
9. Rebelo, S., Pinto, C., Martins, T., Estrada, M., Harrer, N., Alves, P., Sommergruber, W., & Brito, C. (2018). PO-270 3D-3-culture: A tool to unveil macrophage plasticity in the tumour microenvironment. *ESMO Open*, 3, A333. <https://doi.org/10.1136/esmoopen-2018-eacr25.784>
10. Seo, B. R., Chen, X., Ling, L., Song, Y. H., Shimpi, A. A., Choi, S., Gonzalez, J., Sapudom, J., Wang, K., Andresen Eguiluz, R. C., Gourdon, D., Shenoy, V. B., & Fischbach, C. (2020). Collagen microarchitecture mechanically controls myofibroblast differentiation. *Proceedings of the National Academy of Sciences*, 117(21), 11387–11398. <https://doi.org/10.1073/pnas.1919394117>

11. Chen, M. B., Whisler, J. A., Fröse, J., Yu, C., Shin, Y., & Kamm, R. D. (2017). On-chip human microvasculature assay for visualization and quantification of tumor cell extravasation dynamics. *Nature Protocols*, 12(5), 865–880. <https://doi.org/10.1038/nprot.2017.018>
12. Bergers, G., & Song, S. (2005). The role of pericytes in blood-vessel formation and maintenance. *Neuro-Oncology*, 7(4), 452–464. <https://doi.org/10.1215/s1152851705000232>
13. Newman, A. C., Nakatsu, M. N., Chou, W., Gershon, P. D., & Hughes, C. C. W. (2011). The requirement for fibroblasts in angiogenesis: fibroblast-derived matrix proteins are essential for endothelial cell lumen formation. *Molecular Biology of the Cell*, 22(20), 3791–3800. <https://doi.org/10.1091/mbc.e11-05-0393>
14. Lee, S., Ko, J., Park, D., Lee, S. R., Chung, M., Lee, Y., & Jeon, N. L. (2018). Microfluidic-based vascularized microphysiological systems. *Lab on a Chip*, 18(18), 2686–2709. <https://doi.org/10.1039/c8lc00285a>
15. Heil, M., Eitenmüller, I., Schmitz-Rixen, T., & Schaper, W. (2006). Arteriogenesis versus angiogenesis: similarities and differences. *Journal of Cellular and Molecular Medicine*, 10(1), 45–55. <https://doi.org/10.1111/j.1582-4934.2006.tb00290.x>
16. Borasch, K., Richardson, K., & Plendl, J. (2020). Cardiogenesis with a focus on vasculogenesis and angiogenesis. *Anatomia, Histologia, Embryologia*. <https://doi.org/10.1111/ahc.12549>
17. Tompkins, R. (2014). SP0136 Genomic Responses in Mouse Models Poorly Mimic Human Inflammatory Diseases. *Annals of the Rheumatic Diseases*, 73(Suppl 2), 37.3-37. <https://doi.org/10.1136/annrheumdis-2014-eular.1698>
- 18.18.
19. Huh, D. D. (2015). A Human Breathing Lung-on-a-Chip. *Annals of the American Thoracic Society*, 12(Supplement 1), S42–S44. <https://doi.org/10.1513/annalsats.201410-442mg>
20. Tatosian, D. A., & Shuler, M. L. (2009). A novel system for evaluation of drug mixtures for potential efficacy in treating multidrug resistant cancers. *Biotechnology and Bioengineering*, 103(1), 187–198. <https://doi.org/10.1002/bit.22219>
21. Miller, P. G., & Shuler, M. L. (2016). Design and demonstration of a pumpless 14 compartment microphysiological system. *Biotechnology and Bioengineering*, 113(10), 2213–2227. <https://doi.org/10.1002/bit.25989>

22. Wong, K. H., Chan, J. M., Kamm, R. D., & Tien, J. (2012). Microfluidic Models of Vascular Functions. *Annual Review of Biomedical Engineering*, 14(1), 205–230. <https://doi.org/10.1146/annurev-bioeng-071811-150052>
23. Acute respiratory distress syndrome. (2003). *Respiratory Care Clinics*, 9(4), xvii–xviii. [https://doi.org/10.1016/s1078-5337\(03\)00090-x](https://doi.org/10.1016/s1078-5337(03)00090-x)
24. Vulto, P., Podszun, S., Meyer, P., Hermann, C., Manz, A., & Urban, G. A. (2011). Phaseguides: a paradigm shift in microfluidic priming and emptying. *Lab on a Chip*, 11(9), 1596. <https://doi.org/10.1039/c0lc00643b>
25. Bralower, William. (2021, May). *Design, fabrication, and Reduction to practice of milliscale membrane-free organ chip systems*. (Master's Dissertation). Tulane University.
26. S. N. Bhatia and D. E. Ingber, “Microfluidic organs-on-chips,” *Nat. Biotechnol.*, vol. 32, no. 8, Art. no. 8, Aug. 2014, doi: 10.1038/nbt.2989.
27. B. G. Chung *et al.*, “Human neural stem cell growth and differentiation in a gradient-generating microfluidic device,” *Lab. Chip*, vol. 5, no. 4, pp. 401–406, Mar. 2005, doi: 10.1039/B417651K.
28. M. Mondrinos, C. Finck, P. Jones, and P. Lelkes, “Engineering De Novo Assembly of Fetal Pulmonary Organoids,” *Tissue Eng. Part A*, vol. 20, May 2014, doi: 10.1089/ten.TEA.2014.0085.
29. A. W. Orr, B. P. Helmke, B. R. Blackman, and M. A. Schwartz, “Mechanisms of Mechanotransduction,” *Dev. Cell*, vol. 10, no. 1, pp. 11–20, Jan. 2006, doi: 10.1016/j.devcel.2005.12.006.
30. Mondrinos, M. J., Alisafaei, F., Yi, A. Y., Ahmadzadeh, H., Lee, I., Blundell, C., Seo, J., Osborn, M., Jeon, T. J., Kim, S. M., Shenoy, V. B., & Huh, D. (2021). Surface-directed engineering of tissue anisotropy in microphysiological models of musculoskeletal tissue. *Science Advances*, 7(11). <https://doi.org/10.1126/sciadv.abe9446>
31. Allwardt, V., Ainscough, A. J., Viswanathan, P., Sherrod, S. D., McLean, J. A., Haddrick, M., & Pensabene, V. (2020). Translational Roadmap for the Organs-on-a-Chip Industry toward Broad Adoption. *Bioengineering*, 7(3), 112. <https://doi.org/10.3390/bioengineering7030112>
32. Amann, M., & Calbet, J. A. L. (2008). Convective oxygen transport and fatigue. *Journal of Applied Physiology*, 104(3), 861–870. <https://doi.org/10.1152/jappphysiol.01008.2007>
33. Armutcu, F. (2019). Organ crosstalk: the potent roles of inflammation and fibrotic

- changes in the course of organ interactions. *Inflammation Research*, 68(10), 825–839. <https://doi.org/10.1007/s00011-019-01271-7>
34. Huh, D., Matthews, B. D., Mammoto, A., Montoya-Zavala, M., Hsin, H. Y., & Ingber, D. E. (2010). Reconstituting Organ-Level Lung Functions on a Chip. *Science*, 328(5986), 1662–1668. <https://doi.org/10.1126/science.1188302>
 35. Koolwijk, P., Kaijzel, E., van Erck, M., van Hinsbergh, V., & de Maat, M. (2006). Molecular weight fibrinogen variants determine angiogenesis rate in a fibrin matrix in vitro and in vivo. *Vascular Pharmacology*, 45(3), e38. <https://doi.org/10.1016/j.vph.2006.08.174>
 36. Lee, S., Kim, S., Koo, D. J., Yu, J., Cho, H., Lee, H., Song, J. M., Kim, S. Y., Min, D. H., & Jeon, N. L. (2020). 3D Microfluidic Platform and Tumor Vascular Mapping for Evaluating Anti-Angiogenic RNAi-Based Nanomedicine. *ACS Nano*, 15(1), 338–350. <https://doi.org/10.1021/acsnano.0c05110>
 37. Lee, S., & Sung, J. (2017). Microtechnology-Based Multi-Organ Models. *Bioengineering*, 4(4), 46. <https://doi.org/10.3390/bioengineering4020046>
 38. Lin, D. S. Y., Guo, F., & Zhang, B. (2018). Modeling organ-specific vasculature with organ-on-a-chip devices. *Nanotechnology*, 30(2), 024002. <https://doi.org/10.1088/1361-6528/aae7de>
 39. Mandrycky, C. J., Howard, C. C., Rayner, S. G., Shin, Y. J., & Zheng, Y. (2021). Organ-on-a-chip systems for vascular biology. *Journal of Molecular and Cellular Cardiology*, 159, 1–13. <https://doi.org/10.1016/j.yjmcc.2021.06.002>
 40. Maschmeyer, I., Lorenz, A., Ramme, A., Hasenberg, T., Schimek, K., Hübner, J., Lauster, R., & Marx, U. (2015). A microfluidic four-organ-chip for interconnected long-term co-culture of human intestine, liver, skin and kidney equivalents. *Toxicology Letters*, 238(2), S176. <https://doi.org/10.1016/j.toxlet.2015.08.512>
 41. McAleer, C. W., Long, C. J., Elbrecht, D., Sasserath, T., Bridges, L. R., Rumsey, J. W., Martin, C., Schnepfer, M., Wang, Y., Schuler, F., Roth, A. B., Funk, C., Shuler, M. L., & Hickman, J. J. (2019). Multi-organ system for the evaluation of efficacy and off-target toxicity of anticancer therapeutics. *Science Translational Medicine*, 11(497). <https://doi.org/10.1126/scitranslmed.aav1386>
 42. Pollet, A. M., & den Toonder, J. M. (2020). Recapitulating the Vasculature Using Organ-On-Chip Technology. *Bioengineering*, 7(1), 17. <https://doi.org/10.3390/bioengineering7010017>

43. Raghupathi, W., & Raghupathi, V. (2018). An Empirical Study of Chronic Diseases in the United States: A Visual Analytics Approach to Public Health. *International Journal of Environmental Research and Public Health*, *15*(3), 431. <https://doi.org/10.3390/ijerph15030431>
44. Ramadan, Q., & Zourob, M. (2020). Organ-on-a-chip engineering: Toward bridging the gap between lab and industry. *Biomicrofluidics*, *14*(4), 041501. <https://doi.org/10.1063/5.0011583>
45. Schimek, K., Busek, M., Brincker, S., Groth, B., Hoffmann, S., Lauster, R., Lindner, G., Lorenz, A., Menzel, U., Sonntag, F., Walles, H., Marx, U., & Horland, R. (2013). Integrating biological vasculature into a multi-organ-chip microsystem. *Lab on a Chip*, *13*(18), 3588. <https://doi.org/10.1039/c3lc50217a>
46. Sica, A., Allavena, P., & Mantovani, A. (2008). Cancer related inflammation: The macrophage connection. *Cancer Letters*, *267*(2), 204–215. <https://doi.org/10.1016/j.canlet.2008.03.028>
47. Sung, J. H., & Shuler, M. L. (2009). A micro cell culture analog (μ CCA) with 3-D hydrogel culture of multiple cell lines to assess metabolism-dependent cytotoxicity of anti-cancer drugs. *Lab on a Chip*, *9*(10), 1385. <https://doi.org/10.1039/b901377f>
48. Sung, J. H., & Shuler, M. L. (2012). Microtechnology for Mimicking In Vivo Tissue Environment. *Annals of Biomedical Engineering*, *40*(6), 1289–1300. <https://doi.org/10.1007/s10439-011-0491-2>
49. Sung, J. H., Wang, Y. I., Narasimhan Sriram, N., Jackson, M., Long, C., Hickman, J. J., & Shuler, M. L. (2018). Recent Advances in Body-on-a-Chip Systems. *Analytical Chemistry*, *91*(1), 330–351. <https://doi.org/10.1021/acs.analchem.8b05293>
50. Tan, M. L., Ling, L., & Fischbach, C. (2021). Engineering strategies to capture the biological and biophysical tumor microenvironment in vitro. *Advanced Drug Delivery Reviews*, *176*, 113852. <https://doi.org/10.1016/j.addr.2021.113852>
51. Terzic, J., Grivennikov, S., Karin, E., & Karin, M. (2010). Inflammation and Colon Cancer. *Gastroenterology*, *138*(6), 2101–2114. <https://doi.org/10.1053/j.gastro.2010.01.058>

Biography



Gabrielle Fortes was born on July 1st, 1999 in Metairie, LA. She completed her Bachelor of Science in Biomedical Engineering with a minor in Mathematics at Tulane University. She is in the process of completing her Master of Science in Biomedical Engineering at Tulane University through the 4+1 program. Gabrielle's career interests include organ-on-a-chip modeling and orthopedics. After graduation, Gabrielle is planning to move to Boston to continue in the field of organ-on-a-chip modeling. She has accepted a job as a Research Associate at Emulate, Inc. Gabrielle's personal interests include trying new foods and going to the park with her dog, Gigi.